AIMS Mathematics, 11(5): 12866–12894.
DOI: 10.3934/math.2026529
Received: 16 March 2026
Revised: 20 April 2026
Accepted: 27 April 2026
Published: 11 May 2026

https://www.aimspress.com/journal/Math

Research article

A Korteweg–de Vries–Sawada–Kotera–Ramani-type equation: Its integrability and multi-wave solutions

Majid Madadi[1,2], **Kamyar Hosseini**[1,2,3,*], **Farzaneh Alizadeh**[1], **Evren Hincal**[1,4] and **Sekson Sirisubtawee**[5,6,*]

[1] Mathematics Research Center, Near East University, Mersin 10, Nicosia, 99138, Turkey

[2] Research Center of Applied Mathematics, Khazar University, Baku, Azerbaijan

[3] Faculty of Engineering and Natural Sciences, Istanbul Okan University, Istanbul, Turkey

[4] Department of Mathematical Sciences, Saveetha School of Engineering, SIMATS, Chennai-602105, Tamilnadu, India

[5] Department of Mathematics, Faculty of Applied Science, King Mongkut's University of Technology North Bangkok, Bangkok 10800, Thailand

[6] Centre of Excellence in Mathematics, CHE, Si Ayutthaya Road, Bangkok 10400, Thailand

* **Correspondence:** Email: kamyar_hosseini@yahoo.com; sekson.s@sci.kmutnb.ac.th.

Abstract: This paper studies the integrability and nonlinear multi-wave solutions of a Korteweg–de Vries–Sawada–Kotera–Ramani-type (KdV–SKR-type) equation arising in shallow-water wave theory, which is important for modeling nonlinear wave interactions. The integrability of the equation is confirmed by Painlevé analysis, and its bilinear form is subsequently derived using the Bell polynomial (BP) method. Based on the resulting formulation, multi-soliton solutions are constructed via the simplified Hirota method, and the corresponding multi-lump solutions are obtained through the long-wave limit. Furthermore, a Pfaffian framework is developed to construct compact general N-soliton solutions and to systematically generate multi-lump waves within a unified algebraic structure. Various interaction phenomena, including resonant and breather waves, are also derived. The results confirm the integrable nature of the model and reveal rich nonlinear dynamics. The novelty of this work lies in the introduction of the Pfaffian formulation for this equation and the unified construction of its solutions, extending previous studies.

Keywords: KdV–SKR-type equation; bilinearization; integrability; multi-soliton waves; multi-lump waves

Mathematics Subject Classification: 35C08, 35Qxx, 35Q51, 37K40

1. Introduction

Nonlinear partial differential (NLPD) equations serve as essential mathematical models for describing a variety of complex processes that occur in numerous branches of science and engineering, including plasma physics, fluid mechanics, and related disciplines. Because they effectively represent the complex and often non-intuitive behavior of nonlinear systems, NLPD equations have been the focus of extensive theoretical and applied research. In recent years, significant attention has been devoted to exploring diverse classes of nonlinear wave structures of NLPD equations, such as multi-soliton waves, multi-lump waves, etc. For instance, Wazwaz [1] utilized the simplified Hirota method to construct multi-soliton waves for a new fifth-order Painlevé-integrable equation. He and Lü [2] derived multi-lump waves of a three-dimensional Kadomstev–Petviashvili equation through the long-wave limit method. Wang et al. [3] constructed breather and multi-rogue waves of the (3+1)-dimensional Yu–Toda–Sasa–Fukuyama equation using the Hirota bilinear method. Shi et al. [4] obtained new exact solutions, multi-kink solitons, soliton molecules, and lump waves using the Hirota bilinear method and related techniques. In a separate study, Li et al. [5] constructed dark soliton solutions of the coupled complex modified Korteweg–de Vries (KdV) equation using a systematic Pfaffian approach. Additional detailed studies are available in references [6–8].

In addition to these methods, other analytical approaches such as the Darboux [9] and Bäcklund [10] transformations have also been widely used to construct exact solutions of nonlinear partial differential equations. Recently, data-driven techniques, including neural network-based methods, have been applied to obtain approximate soliton solutions [11].

In mathematical physics, a key line of inquiry regarding NLPD equations involves analyzing their potential integrability. While there is no single, universally accepted definition of integrability, an NLPD equation is generally regarded as integrable if it admits certain properties, such as the existence of multi-soliton waves, bilinear Bäcklund transformations, and Lax pairs. These features often indicate that the underlying system can be solved exactly and/or possesses infinite conservation laws, symmetry reductions, and rich dynamical behaviors. Among the various techniques developed for assessing integrability, the Painlevé analysis [12] has demonstrated significant effectiveness. Many studies have investigated the integrability of nonlinear partial differential equations through the application of the Painlevé test. For instance, Yan et al. [13] investigated a thermophoretic motion equation modeling wrinkle propagation in graphene sheets. The Painlevé test confirmed its integrability, leading to the derivation of auto-Bäcklund transformations and multiple kink-wave solutions. Similarly, Chen et al. [14] analyzed a (2+1)-dimensional variable-coefficient combined fourth-order soliton equation relevant to fluid and plasma physics. They verified its Painlevé integrability under certain coefficient constraints and constructed the bilinear form and auto-Bäcklund transformation to obtain various kink and soliton wave solutions. These studies highlight the effectiveness of the Painlevé test in identifying integrable structures and facilitating the derivation of exact solutions in complex nonlinear models.

The BP method offers a unified and efficient framework for investigating NLPD equations. Its origin lies in the classical BP theory introduced in 1934 [15], which provides a systematic way of expressing nonlinear differential relations through polynomial formulations. Building upon this foundation, Lambert et al. [16] extended the concept by introducing generalized BPs, thereby

establishing a coherent methodology for constructing bilinear forms, bilinear Bäcklund transformations, and Lax pairs associated with NLPD equations. In recent decades, the BP method has been extensively employed to study a broad range of NLPD equations in mathematical physics. For example, Hu and Chen [17] utilized the BP method to analyze a non-isospectral, variable-coefficient modified KdV equation, obtaining its bilinear representation and an infinite sequence of conservation laws. Similarly, Wang and Chen [18] applied the BP framework to two higher-order KdV-type equations arising in fluid dynamics, successfully deriving their bilinear forms, Bäcklund transformations, Lax pairs, and conservation laws, thereby confirming their complete integrability. More recently, Hao and Cheng [19] investigated a non-isospectral Kadomtsev–Petviashvili equation using the BP method, deriving its bilinear form, Bäcklund transformation, and Lax pair, and constructing explicit soliton solutions with graphical illustrations. Wang et al. [20] used BPs to construct the bilinear form of the Kairat-II-X-extended equation and derive various exact nonlinear wave solutions. Additional comprehensive investigations into NLPD equations using the BP framework can be found in references [21, 22].

The Pfaffian method provides an efficient algebraic framework for constructing exact solutions of NLPD equations through skew-symmetric matrix structures [23]. Instead of relying on perturbative expansions, this approach expresses the tau function in a compact form that naturally incorporates nonlinear interaction effects. As a result, multi-soliton and multi-lump solutions can be generated systematically within a unified representation. The method not only simplifies higher-order solution construction but also reveals deeper algebraic connections between bilinear equations and integrable hierarchies. The method is particularly used for equations such as the Hirota–Satsuma–Ito [24], modified KdV [5], Boiti–Leon–Manna–Pempinelli [25], and other integrable nonlinear models.

Motivated by the work of Zhu et al. [26] on the formulation of the KdV–SKR equation, this study undertakes a thorough analysis of a KdV–SKR-type equation, i.e.,

$$\begin{aligned} &u_t + \alpha\left(u_x + u_{xxx} + 6uu_x\right) \\ &-\beta\left(u_{xxxxx} + 45u^2u_x + 15uu_y + 15uu_{xxx} + 15u_xu_{xx} + 5u_{xxy} - 5\int u_{yy}dx + 15u_x\int u_y dx\right) = 0. \end{aligned} \tag{1.1}$$

Compared to the integrable KdV–SKR equation, which has wide range of applications in shallow-water wave theory [27], Eq (1.1) incorporates an additional linear term u_x, maintaining the integrability of the model. A substantial body of literature has been devoted to the study of the KdV–SKR equation. Wei et al. [28] derived multi-breather solutions of the KdV–SKR equation by imposing complex conjugate relationships among the parameters in multi-soliton solutions. Subsequently, Chen et al. [29] obtained various hybrid wave solutions of the KdV–SKR equation through the application of different test functions. It can be observed that Eq (1.1) is equivalent to the following system of partial differential equations:

$$\begin{aligned} &u_t + \alpha\left(u_x + u_{xxx} + 6uu_x\right) \\ &-\beta\left(u_{xxxxx} + 45u^2u_x + 15uu_y + 15uu_{xxx} + 15u_xu_{xx} + 5u_{xxy} - 5v_y + 15u_xv\right) = 0, \end{aligned} \tag{1.2a}$$

$$u_y = v_x. \tag{1.2b}$$

When $\alpha = 0$ and $\beta = -1$, Eq (1.2) reduces to the (2+1)-dimensional Sawada–Kotera (SK) equation. On the other hand, when $\beta = 0$ and the additional term u_x is removed, the equation simplifies to the standard KdV equation.

The key goals of the present work are as follows:

First, we investigate the Painlevé integrability properties of the KdV–SKR-type equation and subsequently construct its bilinear representation through the BP method.

Second, based on the obtained bilinear form, we employ the simplified Hirota method to systematically derive exact nonlinear wave solutions, including single- and multi-soliton solutions as well as rationally localized lump waves via the long-wave limit.

Third, we extend the analysis by developing a Pfaffian formulation for the equation. In addition to other frameworks, the Pfaffian method provides a compact algebraic approach for constructing exact solutions of integrable nonlinear models. Unlike the conventional expansion, it represents multi-soliton solutions in a unified form through skew-symmetric structures, allowing general N-soliton solutions to be generated systematically. This formulation naturally encodes nonlinear interactions and offers a more efficient framework for higher-order solution construction.

Moreover, by considering suitable parameter reductions of the general N-soliton solution, Y-type interaction structures and breather waves are further obtained, revealing complex resonance behaviors of nonlinear waves. The Pfaffian technique not only reproduces the soliton solutions obtained via the simplified Hirota method but also enables the construction of lump solutions directly from the Pfaffian structure.

To the best of our knowledge, Pfaffian solutions for the original KdV–SKR equation have not been reported previously, and therefore this work introduces a new representation of its solution structure. We clarify the connection between the considered KdV–SKR-type equation and the KdV–SKR equation through a suitable spatial scaling transformation. This establishes consistency between the solutions obtained here and previously reported results while simultaneously extending them through the Pfaffian construction. Consequently, the present study not only reproduces known multi-soliton and multi-lump solutions but also provides new analytical formulations that broaden the understanding of nonlinear wave interactions within this class of integrable models.

The motivation of this work arises from the need to better understand the integrability and nonlinear wave dynamics of KdV–SKR-type models, which are important in shallow-water wave theory. While the classical KdV–SKR equation has been widely studied, its extended forms still lack a unified and systematic treatment for constructing exact solutions. In this context, the present study provides a comprehensive analysis of a KdV–SKR-type equation by combining integrability analysis with efficient solution methods. The originality of this work lies in the introduction of a Pfaffian formulation for this model, which has not been reported previously for this class of equations. This approach enables a unified construction of N-soliton, lump, and interaction solutions, thereby extending existing results and offering new insights into nonlinear wave behavior.

The paper is organized as follows: Section 2 discusses the integrability analysis and derives the bilinear form of the equation. Section 3 applies the simplified Hirota method and the long-wave limit to construct multi-soliton and multi-lump wave solutions. In Section 4, Pfaffian techniques are introduced to obtain compact multi-soliton representations and to extend the solution framework. Finally, concluding remarks are presented in Section 5.

2. Integrability and bilinear form

Integrability plays a central role in the study of NLPD equations, as integrable systems typically admit exact solutions and stable nonlinear wave interactions. A key indicator of integrability is the existence of a bilinear representation, which provides an efficient framework for analytical investigations. In this section, we analyze the integrability of the KdV–SKR-type model (1.2) using the Painlevé approach and derive its bilinear form via the BP method. The obtained bilinear structure forms the basis for constructing exact wave solutions.

2.1. Painlevé analysis

The integrability of Eq (1.2) is examined using the Weiss–Tabor–Carnevale algorithm [12], a rigorous three-step procedure designed to detect the Painlevé property. The analysis begins with a leading-order behavior study to determine the nature of the solution near the singular manifold, followed by the identification of resonance points where arbitrary functions enter the expansion. Finally, we verify the compatibility conditions at these resonances to ensure the expansion remains consistent. Ultimately, the system is classified as Painlevé integrable if all movable singularities are single-valued, typically appearing as simple poles, thereby precluding the existence of movable branch points or essential singularities.

We posit that the solutions of Eq (1.2) can be represented by generalized Laurent series expansions, given by

$$u = \sum_{b=0}^{\infty} u_b \psi^{b-\gamma_1}, \quad v = \sum_{b=0}^{\infty} v_b \psi^{b-\gamma_2}. \tag{2.1}$$

The parameters γ_1 and γ_2 are positive integers to be identified, and the functions u_b and v_b, with $u_0, v_0 \neq 0$, are analytic in a neighborhood of the noncharacteristic movable singularity manifold specified by $\psi(x, y, t) = 0$.

Equation (1.2) is said to have the Painlevé property provided that its series solution contains a sufficient number of arbitrary functions. By substituting the leading-order expressions

$$u \approx u_0 \psi^{-\gamma_1}, \quad v \approx v_0 \psi^{-\gamma_2} \tag{2.2}$$

into Eq (1.2) and balancing the dominant terms, we obtain

$$u_0 = -2\psi_x^2, \quad v_0 = -2\psi_x\psi_y, \quad \gamma_1 = \gamma_2 = 2. \tag{2.3}$$

To identify the resonance values, namely the powers at which arbitrary functions may appear in the series expansion, we introduce the perturbations

$$u = \frac{u_0}{\psi^2} + \frac{u_1}{\psi} + \sum_{b=2}^{\infty} u_b \psi^{b-2}, \quad v = \frac{v_0}{\psi^2} + \frac{v_1}{\psi} + \sum_{b=2}^{\infty} v_b \psi^{b-2} \tag{2.4}$$

and substitute them into Eq (1.2). Requiring that the coefficients of the terms $\psi^{-7+b}(u_b, v_b)$ and $\psi^{-3+j}(u_b, v_b)$ vanish yields

$$\begin{pmatrix} \beta\psi_x^5\left(-b^5 + 20b^4 - 125b^3 + 250b^2 + 36b - 360\right) & 0 \\ (b-2)\psi_y & -(b-2)\psi_x \end{pmatrix} \begin{pmatrix} u_b \\ v_b \end{pmatrix} = 0. \tag{2.5}$$

By solving Eq (2.5), we can determine the corresponding resonance branches as

$$b = -1, 2, 2, 3, 6, 10. \tag{2.6}$$

The resonance at $b = -1$ naturally reflects the arbitrariness of the singularity manifold $\psi(x, y, t)$. To verify the presence of a sufficient number of arbitrary functions at the resonance points, we substitute the expansions from Eq (2.1) into the equations in (1.2). By collecting the coefficients of ψ^m (ranging from $m = -6$ to 1), we derive the compatibility conditions corresponding to each resonance level. The coefficients u_b are explicitly determined for $b = \{0, 1, 4, 5, 7, 8, 9\}$. Crucially, the coefficients at $b = \{2, 3, 6, 10\}$ remain arbitrary, satisfying the required conditions for the existence of free functions.

As an illustration, the expressions for u_1 and v_1 are

$$u_1 = 2\psi_{x,x}, \quad v_1 = 2\psi_{x,y}. \tag{2.7}$$

Due to their significant length, the remaining expressions are omitted here. Since the resonance conditions are satisfied identically across all levels, we conclude that Eq (1.2) possesses the Painlevé property.

2.2. Bilinear form

Here, by employing logarithmic transformations and BP identities, the KdV–SKR-type Eq (1.1) is converted into its Hirota bilinear form, providing the foundation for applying the direct methods.

Theorem 1. *If*

$$u = 2(\ln \mathfrak{g})_{xx}, \tag{2.8}$$

then the bilinear formalism of Eq (1.1) *is*

$$\Big(D_x D_t + \alpha(D_x^2 + D_x^4) - \beta(D_x^6 + 5D_x^3 D_y - 5D_y^2)\Big)\,\mathfrak{g}\cdot\mathfrak{g} = 0, \tag{2.9}$$

where the Hirota D-operator is defined as

$$D_x^{n_1} D_y^{n_2} D_t^{n_3}(F.G) = \Big(\frac{\partial}{\partial x} - \frac{\partial}{\partial \hat{x}}\Big)^{n_1}\Big(\frac{\partial}{\partial y} - \frac{\partial}{\partial \hat{y}}\Big)^{n_2}\Big(\frac{\partial}{\partial t} - \frac{\partial}{\partial \hat{t}}\Big)^{n_3} \times F(x, y, t)G(\hat{x}, \hat{y}, \hat{t})|_{\hat{x}=x,\hat{y}=y,\hat{t}=t},$$

while n_1, n_2, and n_3 are all non-negative integers satisfying $n_1 + n_2 + n_3 \geq 1$.

Proof. Assume

$$u = c(t)q_{xx} \tag{2.10}$$

and substitute it into Eq (1.1):

$$\begin{aligned} &c(t)q_{xxt} + c'(t)q_{xx} + \alpha\Big(c(t)q_{xxx} + c(t)q_{xxxxx} + 6c^2(t)q_{xx}q_{xxx}\Big) - \beta\Big(c(t)q_{xxxxxxx} + 45c^3(t)q_{xx}^2 q_{xxx} \\ &+ 15c^2(t)q_{xx}q_{xxy} + 15c^2(t)q_{xx}q_{xxxxx} + 15c^2(t)q_{xxx}q_{xxxx} + 5c(t)q_{xxxx,t} - 5c(t)q_{x,yy} + 15c^2(t)q_{xxx}q_{x,y}\Big) = 0. \end{aligned} \tag{2.11}$$

Integrating with respect to x and taking $c(t) = 1$ yields

$$q_{xt} + \alpha(q_{xx} + q_{xxxx} + 3q_{xx}^2) - \beta(q_{xxxxxx} + 15q_{xx}q_{x,y} + 5q_{xxx,y} + 15q_{xx}^3 - 5q_{yy} + 15q_{xx}q_{xxxx}) = 0. \tag{2.12}$$

Equation (2.12) in P-polynomial form is

$$P_{x,t}(q) + \alpha(P_{2x}(q) + P_{4x}(q)) - \beta(P_{6x}(q) + 5P_{3x,y}(q) - 5P_{2y}(q)) = 0. \tag{2.13}$$

Using

$$q = 2\ln \mathfrak{g} \quad \Longleftrightarrow \quad u = q_{xx} = 2(\ln \mathfrak{g})_{xx}, \tag{2.14}$$

we obtain (2.9). □

3. Multi-soliton and multi-lump wave solutions

Once the bilinear form is obtained, systematic procedures can be applied for constructing exact nonlinear wave solutions. In this section, we derive multi-soliton solutions of the governing model using the simplified Hirota method and then obtain their corresponding multi-lump solutions via the long-wave limit.

3.1. Multi-soliton waves

Solitons are stable traveling waves formed by the balance of nonlinearity and dispersion, maintaining their shape and velocity even after interactions, a hallmark of integrable systems. In shallow-water environments, these waves propagate over long distances without distortion. The derived multi-soliton solutions demonstrate elastic collisions where waves re-emerge unchanged, highlighting the energy-preserving nature and robustness of nonlinear wave patterns in physical media.

Assume

$$u = e^{\theta_i}, \qquad \theta_i = k_i\,(x + r_i y + \omega_i t) + \zeta_i, \quad i \in \mathbb{N}$$

and substitute it into the linearized equation

$$u_t + \alpha(u_x + u_{xxx}) - \beta(u_{xxxxx} + 5u_{xxy} - 5\int u_{yy}dx) = 0. \tag{3.1}$$

This gives

$$\left(\omega_i + \alpha\left(k_i^2 + 1\right) - \beta\left(k_i^4 + 5k_i^2 r_i - 5r_i^2\right)\right)k_i e^{k_i(x + r_i y + \omega_i t) + \zeta_i} = 0. \tag{3.2}$$

Hence, the dispersion relation is

$$\omega_i = -\alpha\left(k_i^2 + 1\right) + \beta\left(k_i^4 + 5k_i^2 r_i - 5r_i^2\right). \tag{3.3}$$

Consequently, the phase variable becomes

$$\theta_i = k_i\left(x + r_i y - \left(\alpha\left(k_i^2 + 1\right) - \beta\left(k_i^4 + 5k_i^2 r_i - 5r_i^2\right)\right)t\right) + \zeta_i. \tag{3.4}$$

The single-soliton solution can be obtained as

$$u = 2(\ln \mathfrak{g}_1)_{xx}, \qquad \mathfrak{g} = 1 + e^{\theta_1}. \tag{3.5}$$

To derive the two-soliton solution, we assume that the tau function contains two independent phase variables in the form

$$\mathfrak{g}_2 = 1 + e^{\theta_1} + e^{\theta_2} + e^{\theta_1+\theta_2+a_{12}}, \tag{3.6}$$

where the coefficient a_{12} characterizes the interaction between the two elementary solitons. Substituting this expression into the bilinear equation (2.9) and applying some operations determines $e^{a_{12}}$. The resulting solution describes the elastic interaction of two solitons, each preserving its amplitude and velocity after collision, which is a fundamental property of integrable systems.

Following the same procedure, the three-soliton solution is obtained by introducing a third exponential mode. The tau function then takes the form

$$\mathfrak{g}_3 = 1 + \sum_{i=1}^{3} e^{\theta_i} + \sum_{1\le i<j\le 3} e^{\theta_i+\theta_j+a_{ij}} + e^{\theta_1+\theta_2+\theta_3+a_{12}+a_{13}+a_{23}}. \tag{3.7}$$

The product term $a_{12}a_{13}a_{23}$ guarantees consistency of the bilinear equation and reflects the factorized structure of multi-soliton interactions. Notably, no higher-order interaction parameters appear beyond pairwise coefficients, confirming the integrable nature of the equation.

This construction naturally generalizes to the N-soliton case. By introducing N independent phase variables, the tau function can be expressed as a finite sum over all possible combinations of exponential modes. Each term represents nonlinear interactions among solitons, while the interaction coefficients depend only on pairwise parameter relations. Finally, the general N-soliton solution has the form

$$u_N = 2(\ln \mathfrak{g}_N)_{xx}, \tag{3.8}$$

with

$$\mathfrak{g}_N = \sum_{\mu=0,1} \exp\left(\sum_{i=1}^{N} \mu_i\theta_i + \sum_{1\le i<j}^{N} \mu_i\mu_j a_{ij}\right), \tag{3.9}$$

where θ_i and $e^{a_{ij}}$ are given by

$$\theta_i = k_i\left(x + r_i y - \left(\alpha\left(k_i^2+1\right) - \beta\left(k_i^4 + 5k_i^2 r_i - 5r_i^2\right)\right)t\right) + \zeta_i, \quad e^{a_{ij}} = \frac{p_1}{p_2}, \tag{3.10}$$

with p_1 and p_2 defined as

$$\begin{aligned} p_1 &= \left(-5k_i^4 + 15k_i^3k_j - 5\left(4k_j^2 + 2r_i + r_j\right)k_i^2 + 15k_j\left(k_j^2 + r_i + r_j\right)k_i - 5k_j^4 - 5\left(r_i + 2r_j\right)k_j^2 - 5\left(r_i - r_j\right)^2\right)\beta \\ &\quad + 3\alpha\left(k_i - k_j\right)^2, \\ p_2 &= \left(-5k_i^4 - 15k_i^3k_j - 5\left(4k_j^2 + 2r_i + r_j\right)k_i^2 - 15k_j\left(k_j^2 + r_i + r_j\right)k_i - 5k_j^4 - 5\left(r_i + 2r_j\right)k_j^2 - 5\left(r_i - r_j\right)^2\right)\beta \\ &\quad + 3\alpha\left(k_i + k_j\right)^2. \end{aligned}$$

Here, k_i, r_i, and ζ_i ($i = 1, 2, \ldots, N$) denote arbitrary parameters. The notation $\sum_{\mu=0,1}$ represents the summation over all possible configurations of μ_i, where each μ_i independently takes the value 0 or 1 for $i = 1, 2, \ldots, N$. Furthermore, the symbol $\sum_{1\le i<j}^{N}$ indicates a summation taken over every distinct pair (i, j) selected from the index set $\{1, 2, \ldots, N\}$ subject to the ordering condition $1 \le i < j$.

The first three soliton solutions are presented using three-dimensional surface plots together with their corresponding density projections in Figure 1. Figure 1 (a) shows the single-soliton case, characterized by a localized ridge structure. In this case, the wave maintains a stable localized profile, confirming its particle-like behavior. Figure 1 (b) illustrates the two-soliton interaction, where nonlinear effects produce a cross-shaped pattern and localized amplification at the intersection. In this interaction, the waves undergo a collision characterized by temporary amplitude enhancement at the interaction region, after which they recover their original shapes and velocities. Figure 1 (c) displays the three-soliton solution, which demonstrates more complex interaction patterns while still preserving the fundamental property of elastic interactions. These observations highlight the stability and robustness of soliton solutions in the considered model. The surface plots depict the amplitude of the wave profile $u(x, y, t)$, while the density plots emphasize spatial localization. Parameter values are specified for each panel.

It is worth mentioning that the amplitude of the ith soliton is given by $\frac{1}{2}k_i^2$. Accordingly, Eq (1.1) admits only bright soliton solutions and does not support dark (depression-type) solitons.

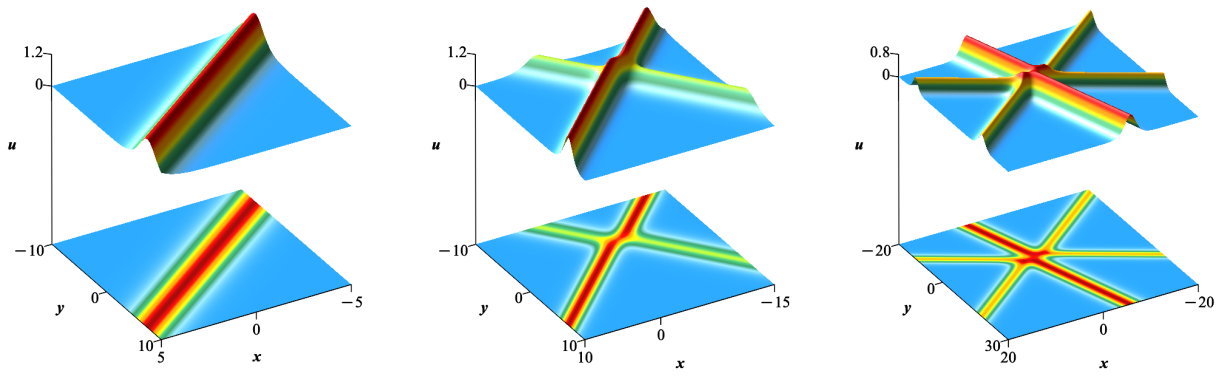

(a) **(b)** **(c)**

Figure 1. The one-, two-, and three-soliton solutions (3.5)–(3.7). Three-dimensional surface plots of the wave profile $u(x, y, t)$. The parameters are set as **(a)** $\alpha = 1, \beta = 1, k_1 = \frac{3}{2}, r_1 = -\frac{2}{3}$, **(b)** $\alpha = 1, \beta = 1, k_1 = 1, k_2 = \frac{3}{2}, r_1 = 1, r_2 = -\frac{5}{4}, \zeta_1 = 10, \zeta_2 = 0$, **(c)** $\alpha = 1, \beta = 1, k_1 = 1, k_2 = 1, k_3 = \frac{5}{4}, r_1 = -1, r_2 = \frac{27}{20}, r_3 = \frac{1}{4}, \zeta_1 = \zeta_2 = \zeta_3 = 1$ when $t = 0$.

3.2. Multi-lump waves

Lump waves are non-singular, rationally localized solutions that decay algebraically in all spatial directions, unlike exponentially decaying solitons. Physically, they model localized wave packets with high-amplitude concentration in dispersive media like shallow water. Their smooth spatial decay effectively describes transient wave focusing and peak formation, while their interactions reveal complex superposition effects and the development of high-intensity regions. Here, lump solutions of the KdV–SKR-type equation are derived by applying the long-wave limit to soliton solutions, leading to explicit single- and multi-lump wave structures.

Assuming $e^{\zeta_1} = -1$ and $e^{\zeta_2} = -1$ results in a double-soliton wave of the KdV–SKR-type equation

as follows:

$$u = 2(\ln \mathfrak{g})_{xx}, \qquad \mathfrak{g} = 1 - e^{\xi_1} - e^{\xi_2} + e^{\xi_1+\xi_2+a_{12}}, \tag{3.11}$$

where

$$\xi_i = k_i \left(x + r_i y - \left(\alpha \left(k_i^2 + 1\right) - \beta \left(k_i^4 + 5k_i^2 r_i - 5r_i^2\right)\right)t\right) \tag{3.12}$$

and $e^{a_{12}}$ can be found from (3.10). Through applying the Taylor series, we find

$$\begin{aligned} \mathfrak{g} = &-1 - k_1\bar{\theta}_1 - k_2\bar{\theta}_2 - \frac{1}{2}k_1^2\bar{\theta}_1^2 - \frac{1}{2}k_2^2\bar{\theta}_2^2 \\ &+ \left(1 + k_1\bar{\theta}_1 + k_2\bar{\theta}_2 + \frac{1}{2}k_1^2\bar{\theta}_1^2 + k_1k_2\bar{\theta}_1\bar{\theta}_2 + \frac{1}{2}k_2^2\bar{\theta}_2^2\right)(1 + k_1k_2B_{12}) + \cdots, \end{aligned} \tag{3.13}$$

where

$$\bar{\theta}_i = x + r_i y - (5\beta r_i^2 + \alpha)t, \quad i = 1, 2, \tag{3.14}$$

$$B_{12} = -\frac{6(5\beta r_1 + 5\beta r_2 - 2\alpha)}{5\beta(r_1 - r_2)^2}. \tag{3.15}$$

After simplifying, Eq (3.13) can be written as

$$\mathfrak{g} = k_1k_2(\bar{\theta}_1\bar{\theta}_2 + B_{12}) + O(k). \tag{3.16}$$

Now, a single-lump wave (when $k_i \to 0$ for $i = 1, 2$) to the KdV–SKR-type equation is derived as

$$u_1 = 2(\ln \mathfrak{g}_1)_{xx}, \qquad \mathfrak{g}_1 = \bar{\theta}_1\bar{\theta}_2 + B_{12}, \tag{3.17}$$

where θ_i and B_{12} are given in (3.14) and (3.15), respectively, for $r_2 = r_1^*$.

We are capable of representing the double-lump wave to the KdV–SKR-type equation as follows:

$$\begin{aligned} \mathfrak{g}_2 = &\bar{\theta}_1\bar{\theta}_2\bar{\theta}_3\bar{\theta}_4 + B_{12}\bar{\theta}_3\bar{\theta}_4 + B_{13}\bar{\theta}_2\bar{\theta}_4 + B_{14}\bar{\theta}_2\bar{\theta}_3 + B_{23}\bar{\theta}_1\bar{\theta}_4 + B_{24}\bar{\theta}_1\bar{\theta}_3 + B_{34}\bar{\theta}_1\bar{\theta}_2 + B_{12}B_{34} \\ &+ B_{13}B_{24} + B_{14}B_{23}, \end{aligned} \tag{3.18}$$

with

$$\bar{\theta}_i = x + r_i y - (5\beta r_i^2 + \alpha)t, \quad i = 1, \ldots, 4, \tag{3.19}$$

$$B_{ij} = -\frac{6(5\beta r_i + 5\beta r_j - 2\alpha)}{5\beta(r_i - r_j)^2}, \qquad i < j, \tag{3.20}$$

$$r_1 = r_3^*, \quad r_2 = r_4^*. \tag{3.21}$$

Accordingly, we can summarize that the lump-type solutions of Eq (1.1) can be obtained from the the N-soliton expression (3.9) by choosing $N = 2L$, setting $\zeta_i = \mathbf{i}\,\pi$, and subsequently taking the long-wave limit $k_i \to 0$ (applying Taylor expansion). Under this procedure, the Lth-order lump solutions are derived in the form

$$u_N = 2(\ln \mathfrak{g}_N)_{xx}, \tag{3.22}$$

where

$$\mathfrak{g}_N = \prod_{i=1}^{N} \bar{\theta}_i + \frac{1}{2} \sum_{i,j}^{N} \left(B_{ij} \prod_{l \neq i,j}^{N} \bar{\theta}_l \right) + \cdots + \frac{1}{L!\, 2^L} \sum_{i,j,\ldots,n,q}^{N} \left(\underbrace{B_{ij} B_{lm} \cdots B_{nq}}_{L} \prod_{p \neq i,j,\ldots,n,q}^{N} \bar{\theta}_p \right) + \cdots . \tag{3.23}$$

The phase variables and interaction coefficients are defined by

$$\bar{\theta}_i = x + r_i y - (5\beta r_i^2 + \alpha)t, \tag{3.24}$$

$$B_{ij} = -\frac{6(5\beta r_i + 5\beta r_j - 2\alpha)}{5\beta (r_i - r_j)^2}, \qquad i < j, \tag{3.25}$$

$$r_{L+i} = r_i^*, \quad L = \frac{N}{2}, \quad i = 1, 2, \ldots, L, \tag{3.26}$$

where the parameters satisfy $\beta \neq 0$ and $r_i \neq r_j$. The notation $\sum_{i,j,\ldots,n,q}^{N}$ represents summation over all possible combinations of indices $i, j, \ldots, n, q$ selected from the set $\{1, 2, \ldots, N\}$ such that all indices are mutually distinct.

Utilizing (3.23), higher-order lump waves can be generated. Figure 2 presents one-, two-, and three-lump solutions through three-dimensional plots of the wave profile $u(x, y, t)$, demonstrating their spatial localization and algebraic decay. Figure 2 (a) shows a single localized lump that decays smoothly in space. Figure 2 (b) displays two separated lumps, while Figure 2 (c) shows three lumps, illustrating the formation of multiple localized wave structures. The single lump appears as an isolated peak with smooth decay in all directions, while multiple lump solutions exhibit interactions that lead to the formation of several localized peaks. Unlike soliton interactions, lump waves do not exhibit simple elastic behavior; instead, their superposition results in more intricate structures and localized amplitude variations. These features provide insight into the formation of highly concentrated wave patterns in nonlinear dispersive systems.

In what follows, we adopt an alternative but closely related approach based on the Pfaffian technique. We reproduce the previously obtained solutions within a unified algebraic framework. Unlike the above approaches, Pfaffians offer a compact representation of multi-soliton solutions, naturally encoding interaction structures through skew-symmetric matrices. This formulation simplifies the construction of higher-order solutions and provides a more systematic path toward general N-soliton expressions.

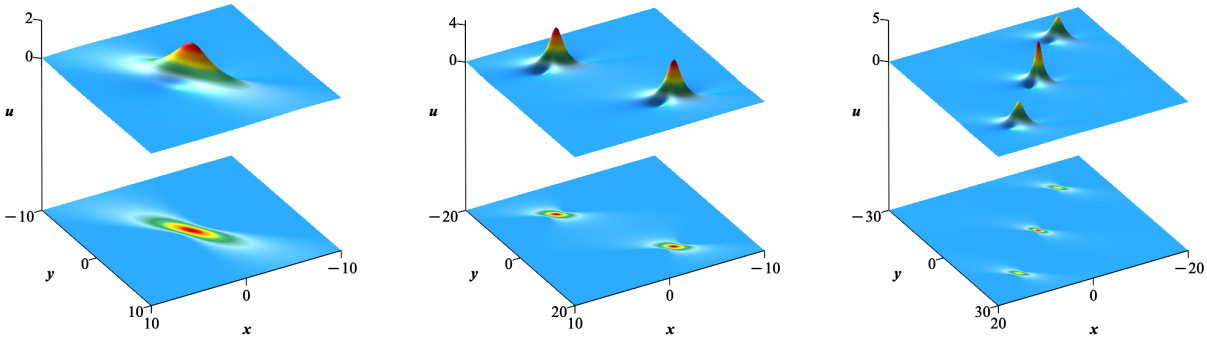

(a) **(b)** **(c)**

Figure 2. The one-, two-, and three-lump solutions. Three-dimensional surface plots of the wave profile $u(x, y, t)$. The parameters are set as **(a)** $r_1 = \frac{1}{2} + \frac{3}{4}\mathbf{i}$. **(b)** $r_1 = r_4^* = \frac{1}{2} + \frac{3}{4}\mathbf{i}, r_2 = r_3^* = \frac{1}{4} + \mathbf{i}$. **(c)** $r_1 = r_4^* = \frac{1}{2} + \frac{3}{4}\mathbf{i}, r_2 = r_5^* = \frac{1}{4} + \frac{3}{4}\mathbf{i}, r_3 = r_6^* = \frac{2}{3} + \frac{3}{4}\mathbf{i}$.

4. Pfaffian solutions

Pfaffian structures provide a compact algebraic representation of multi-soliton solutions in integrable systems. Arising from skew-symmetric matrices, Pfaffians extend determinant formulations and naturally satisfy bilinear equations. The Pfaffian representation not only provides a compact mathematical structure but also offers a unified physical interpretation of nonlinear wave interactions. Through this framework, complex wave phenomena such as resonant interactions, breather formations, and fission–fusion processes can be described systematically. These behaviors reflect realistic physical scenarios in which wave energy is redistributed among interacting modes, leading to the emergence of diverse localized structures.

In this section, the Pfaffian framework is introduced for the KdV–SKR-type equation, and the corresponding tau function is constructed to generate multi-soliton solutions in a unified manner.

Let (i, j) denote the entries of a skew-symmetric matrix (or 2-forms) satisfying $(i, j) = -(j, i)$ and $(i, i) = 0$. The Nth-order Pfaffian is defined by

$$\tau_N = (1, 2, 3, \ldots, 2N), \tag{4.1}$$

with the recursive expansion, analogous to the Laplace expansion of a determinant,

$$(1, 2, \ldots, 2N) = \sum_{j=2}^{2N} (-1)^j (1, j)\,(2, 3, \ldots, \widehat{j}, \ldots, 2N), \tag{4.2}$$

where $\widehat{j}$ indicates omission of the index j. Here, $(1, j)$ plays the role of a matrix entry, $(-1)^j$ is the cofactor sign, and the remaining term is a Pfaffian of order $N - 1$. For example, $\tau_1 = (1, 2)$, and for $N = 2$,

$$\tau_2 = (1, 2, 3, 4) = (1, 2)(3, 4) - (1, 3)(2, 4) + (1, 4)(2, 3), \tag{4.3}$$

illustrating the alternating–sign structure of the expansion.

Here, the determinant in the previous discussion is taken of an antisymmetric matrix with entries (i, j) defined by

$$(i, j) = c_{i,j}\frac{k_i - k_j}{k_i + k_j} + \int^x D_x\psi_i.\psi_j dx, \tag{4.4}$$

where k_i and k_j are given parameters, ψ_i and ψ_j are real functions depending on the variables (x, y, t), and D_x is Hirota's bilinear operator.

Specifically, we define the coefficients

$$c_{2i-1,2i} = c_{2i,2i-1} = 1, \quad i = 1, 2, \ldots, N, \tag{4.5}$$

while all other coefficients $c_{i,j}$ are set to zero. Moreover, the functions ψ_i and ψ_j satisfy the linear partial differential equations

$$\psi_{i,y} = \frac{\alpha}{5\beta}\psi_{i,x} - \psi_{i,xxx}, \tag{4.6a}$$

$$\psi_{i,t} = \left(-\frac{\alpha^2}{5\beta} - \alpha\right)\psi_{i,x} + 2\alpha\psi_{i,xxx} - 9\beta\psi_{i,xxxxx}. \tag{4.6b}$$

To prove that the Pfaffian solves the bilinear equation (2.9), one first computes the derivatives of the entries (i, j) using the linear system (4.6). These derivatives are then substituted into the bilinear equation, which verifies the solution. The detailed calculations are omitted here for brevity; the reader is referred to [30, 31] for complete derivations.

4.1. Soliton solutions from the Pfaffian method perspective

Soliton solutions of the KdV–SKR-type equation can be constructed using the Pfaffian $\tau_N = (1, 2, \ldots, 2N)$ introduced above. To this end, the entries (i, j) of the antisymmetric matrix are expressed in terms of real functions $\phi_i(x, y, t)$ and coefficients $c_{i,j}$. For soliton solutions, we take ψ_i and ψ_j in the form of plane waves

$$\psi_i = e^{\phi_i}, \qquad \psi_j = e^{\phi_j}, \tag{4.7}$$

with

$$\phi_i = k_i x + \left(\frac{\alpha k_i}{5\beta} - k_i^3\right)y + \Big(-\frac{k_i\alpha^2}{5\beta} - k_i\alpha + 2\alpha k_i^3 - 9\beta k_i^5\Big)t + \zeta_i, \tag{4.8a}$$

$$\phi_j = k_j x + \left(\frac{\alpha k_j}{5\beta} - k_j^3\right)y + \Big(-\frac{k_j\alpha^2}{5\beta} - k_j\alpha + 2\alpha k_j^3 - 9\beta k_j^5\Big)t + \zeta_j, \tag{4.8b}$$

where k_i and ζ_i are free parameters.

By substituting the expression (4.7) into Eq (4.4), we obtain

$$(i, j) = c_{i,j}\frac{k_i - k_j}{k_i + k_j} + \frac{k_i - k_j}{k_i + k_j}\psi_i\psi_j. \tag{4.9}$$

Moreover, inserting the expression (4.9) into Eq (4.1) yields the N-soliton solution of the KdV–SKR-type equation (1.1), which can be expressed as

$$u = 2[\ln \tau_N]_{xx}. \tag{4.10}$$

According to the obtained solution, the field u represents an N-soliton configuration. Each individual soliton is associated with a pair of wave numbers (k_{2i-1}, k_{2i}) for $i = 1, 2, \ldots, N$. The amplitude and spatial location of each soliton are determined by these parameters, which govern the shape and propagation properties of the corresponding soliton waves.

The space-time evolution of each soliton is governed by

$$t = \frac{5\beta\left(k_{2i-1}+k_{2i}\right)\, x + \left(\alpha\left(k_{2i-1}+k_{2i}\right) - 5\beta\left(k_{2i-1}^3 + k_{2i}^3\right)\right) y + 5\beta\left(\zeta_{2i-1}+\zeta_{2i}\right)}{45\beta^2\left(k_{2i-1}^5 + k_{2i}^5\right) + 5\alpha\beta\left(k_{2i-1}+k_{2i}-2k_{2i-1}^3-2k_{2i}^3\right) + \alpha^2\left(k_{2i-1}+k_{2i}\right)}. \tag{4.11}$$

The amplitude of each soliton is given by

$$A_i = \frac{\left(k_{2i-1}+k_{2i}\right)^2}{2}. \tag{4.12}$$

We now focus on using the general solution (4.10) to construct soliton solutions for $N = 1, ..., 4$.

One-soliton: The simplest scenario occurs when we set $N = 1$ in the Pfaffian solution (4.1). In this case, it reduces to the following form:

$$\tau_1 = \frac{k_1 - k_2}{k_1 + k_2}\left(1 + e^{\phi_1+\phi_2}\right). \tag{4.13}$$

Consequently, the one-soliton solution is obtained as

$$u_1 = \frac{\left(k_1+k_2\right)^2}{2}\,\mathrm{sech}\left(\frac{\phi_1+\phi_2}{2}\right)^2. \tag{4.14}$$

Here, k_1 and k_2 are free parameters, and ϕ_1 and ϕ_2 are given by (4.8). The evolution dynamics of the wave are shown in Figure 3, along with its amplitude and soliton direction.

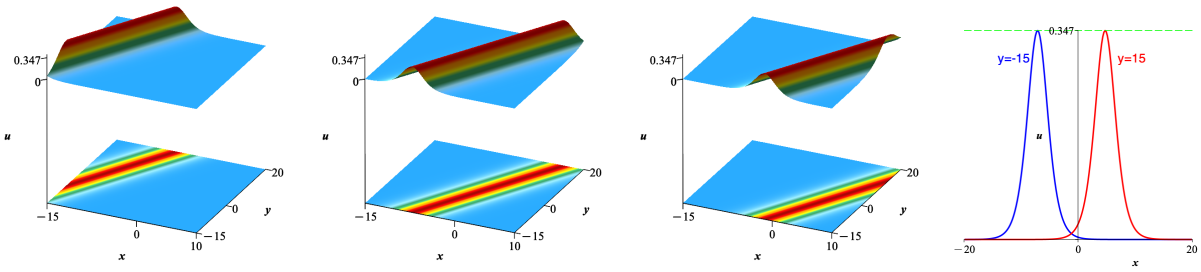

(a) $t = -400$ **(b)** $t = 0$ **(c)** $t = 200$ **(d)** $t = 0$

Figure 3. Evolution of a single-soliton solution (4.14) for parameters $\alpha = 1, \beta = -1, k_1 = \frac{1}{2}, k_2 = \frac{1}{3}, \zeta_1 = 0, \zeta_2 = 1$. Three-dimensional surface plots of the wave profile $u(x, y, t)$ are shown at **(a)** $t = -400$, **(b)** $t = 0$, and **(c)** $t = 200$, illustrating the stable propagation of the soliton without change in shape. **(d)** displays the corresponding one-dimensional cross-sections at $t = 0$ for fixed $y = \pm 15$. The soliton has constant amplitude 0.3472 and propagates along the trajectory $x = \frac{7t}{240} + \frac{71y}{180} - \frac{6}{5}$.

Two-soliton: For $N = 2$, the Pfaffian expression takes the form

$$\tau_2 = \frac{(k_1 - k_2)(k_3 - k_4)(1 + e^{\phi_1+\phi_2})(1 + e^{\phi_3+\phi_4})}{(k_1 + k_2)(k_3 + k_4)} - \frac{2(k_1 - k_2)(k_3 - k_4)(k_1k_2 + k_3k_4)e^{\phi_1+\phi_2+\phi_3+\phi_4}}{(k_1 + k_3)(k_1 + k_4)(k_2 + k_3)(k_2 + k_4)}. \tag{4.15}$$

Substituting this expression into Eq (4.10), we obtain the two-soliton solution. The solution at different times is illustrated in Figure 4. The characteristics of each wave are also indicated in the figure.

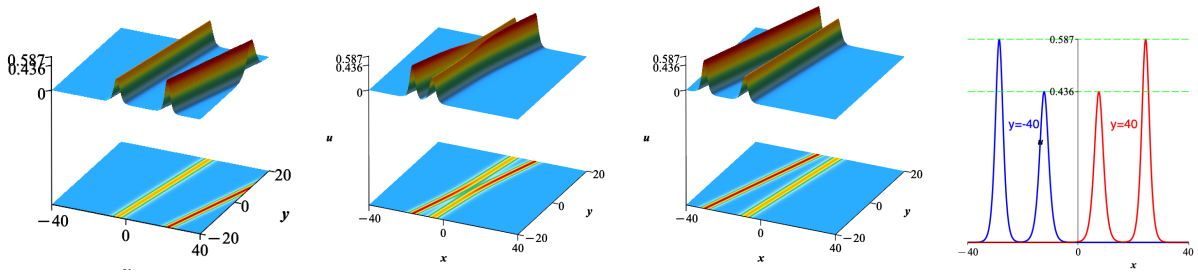

(a) $t = -5$ **(b)** $t = 0$ **(c)** $t = 2$ **(d)** $t = 0$

Figure 4. Evolution of a two-soliton solution (4.15) for parameters $\alpha = \frac{1}{2}, \beta = -2, k_1 = \frac{1}{3}, k_2 = \frac{3}{5}, k_3 = \frac{5}{6}, k_4 = \frac{1}{4}, \zeta_1 = 5, \zeta_2 = 0, \zeta_3 = 5, \zeta_4 = 0$. Three-dimensional surface plots of the wave profile $u(x, y, t)$ are shown at **(a)** $t = -5$, **(b)** $t = 0$, and **(c)** $t = 2$, demonstrating the interaction and stable propagation of two solitons. **(d)** shows the corresponding one-dimensional cross-sections at $t = 0$ for fixed $y = \pm 40$. The amplitudes of the first and second solitons are 0.435 and 0.586, respectively, propagating along the trajectories $x = -\frac{20627t}{15000} + \frac{289y}{900} - \frac{75}{14}$ and $x = -\frac{4331t}{640} + \frac{431y}{720} - \frac{60}{13}$.

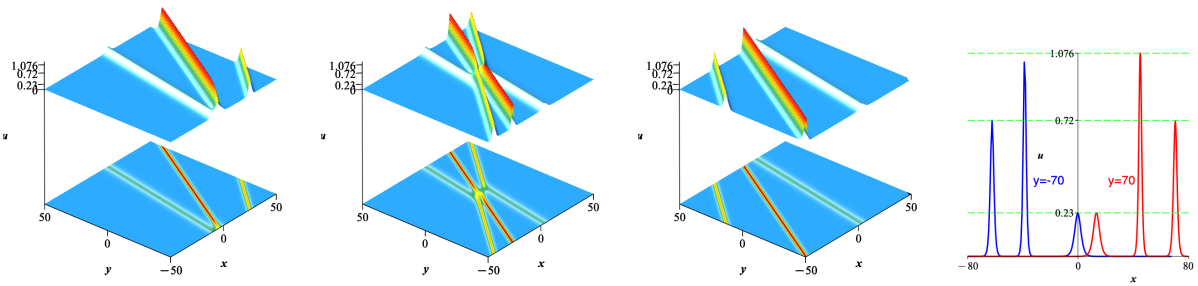

(a) $t = -4$ **(b)** $t = 0$ **(c)** $t = 4$ **(d)** $t = 0$

Figure 5. Evolution of a three-soliton solution (4.16) for parameters $\alpha = \frac{1}{2}, \beta = -2, k_1 = \frac{1}{5}, k_2 = 1, k_3 = \frac{1}{4}, k_4 = \frac{3}{7}, k_5 = \frac{2}{3}, k_6 = \frac{4}{5}, \zeta_1 = \zeta_2 = \zeta_3 = \zeta_4 = \zeta_5 = \zeta_6 = 0$. Three-dimensional surface plots of the wave profile $u(x, y, t)$ are shown at **(a)** $t = -5$, **(b)** $t = 0$, and **(c)** $t = 2$, demonstrating the interaction and stable propagation of three solitons. **(d)** shows the corresponding one-dimensional cross-sections at $t = 0$ for fixed $y = \pm 70$. The amplitudes of the first, second, and third solitons are 0.72, 0.23, and 1.075, respectively, propagating along the trajectories $x = -\frac{76849t}{5000} + \frac{89y}{100}$, $x = -\frac{112881t}{1536640} + \frac{741y}{3920}$ and $x = -\frac{28569t}{5000} + \frac{541y}{900}$.

Similarly, for $N = 3, 4$, the expressions for τ_N are given below. Moreover, Figures 5 and 6 illustrate the dynamical behavior of the three- and four-soliton solutions, respectively.

$$\begin{aligned}\tau_3 &= \Lambda_{1,2,3,4,5,6}\Big[1 + e^{\phi_1+\phi_2} + e^{\phi_3+\phi_4} + e^{\phi_5+\phi_6} + \Lambda_{1,2,3,4}e^{\phi_1+\phi_2+\phi_3+\phi_4} + \Lambda_{1,2,5,6}e^{\phi_1+\phi_2+\phi_5+\phi_6} \\ &\quad + \Lambda_{3,4,5,6}e^{\phi_3+\phi_4+\phi_5+\phi_6} + (\Lambda_{1,2,3,4}\Lambda_{1,2,5,6}\Lambda_{3,4,5,6})e^{\phi_1+\phi_2+\phi_3+\phi_4+\phi_5+\phi_6}\Big], \qquad (4.16)\\ \tau_4 &= \Lambda_{1,2,3,4,5,6,7,8}\Big[1 + e^{\phi_1+\phi_2} + e^{\phi_3+\phi_4} + e^{\phi_5+\phi_6} + e^{\phi_7+\phi_8} + \Lambda_{1,2,3,4}e^{\phi_1+\phi_2+\phi_3+\phi_4} + \Lambda_{1,2,5,6}e^{\phi_1+\phi_2+\phi_5+\phi_6} \\ &\quad + \Lambda_{1,2,7,8}e^{\phi_1+\phi_2+\phi_7+\phi_8} + \Lambda_{3,4,5,6}e^{\phi_3+\phi_4+\phi_5+\phi_6} + \Lambda_{3,4,7,8}e^{\phi_3+\phi_4+\phi_7+\phi_8} + \Lambda_{5,6,7,8}e^{\phi_5+\phi_6+\phi_7+\phi_8} \qquad (4.17)\\ &\quad + \Lambda_{1,2,3,4,5,6}e^{\phi_1+\phi_2+\phi_3+\phi_4+\phi_5+\phi_6} + \Lambda_{1,2,3,4,7,8}e^{\phi_1+\phi_2+\phi_3+\phi_4+\phi_7+\phi_8} + \Lambda_{1,2,5,6,7,8}e^{\phi_1+\phi_2+\phi_5+\phi_6+\phi_7+\phi_8} \\ &\quad + \Lambda_{3,4,5,6,7,8}e^{\phi_3+\phi_4+\phi_5+\phi_6+\phi_7+\phi_8} + \Lambda_{1,2,3,4,5,6,7,8}e^{\phi_1+\phi_2+\phi_3+\phi_4+\phi_5+\phi_6+\phi_7+\phi_8}\Big],\end{aligned}$$

where

$$\begin{aligned}&\Lambda_{1,2,3,4} = \frac{(k_1-k_3)(k_1-k_4)(k_2-k_3)(k_2-k_4)}{(k_1+k_3)(k_1+k_4)(k_2+k_3)(k_2+k_4)}, \quad \Lambda_{1,2,5,6} = \frac{(k_5-k_1)(k_5-k_2)(k_6-k_1)(k_6-k_2)}{(k_1+k_5)(k_1+k_6)(k_2+k_5)(k_2+k_6)},\\ &\Lambda_{3,4,5,6} = \frac{(k_5-k_3)(k_5-k_4)(k_6-k_3)(k_6-k_4)}{(k_3+k_5)(k_3+k_6)(k_4+k_5)(k_4+k_6)}, \quad \Lambda_{1,2,7,8} = \frac{(k_1-k_7)(k_1-k_8)(k_2-k_7)(k_2-k_8)}{(k_1+k_7)(k_1+k_8)(k_2+k_7)(k_2+k_8)},\\ &\Lambda_{3,4,7,8} = \frac{(k_3-k_7)(k_3-k_8)(k_4-k_7)(k_4-k_8)}{(k_3+k_7)(k_3+k_8)(k_4+k_7)(k_4+k_8)}, \quad \Lambda_{5,6,7,8} = \frac{(k_5-k_7)(k_5-k_8)(k_6-k_7)(k_6-k_8)}{(k_5+k_7)(k_5+k_8)(k_6+k_7)(k_6-k_8)},\\ &\Lambda_{1,2,3,4,5,6} = \frac{(k_1-k_2)(k_3-k_4)(k_5-k_6)}{(k_1+k_2)(k_3+k_4)(k_5+k_6)}, \quad \Lambda_{1,2,3,4,5,6,7,8} = \frac{(k_1-k_2)(k_3-k_4)(k_5-k_6)(k_7-k_8)}{(k_1+k_2)(k_3+k_4)(k_5+k_6)(k_7+k_8)},\\ &\Lambda_{1,2,3,4,7,8} = \Lambda_{1,2,3,4}\Lambda_{1,2,7,8}\Lambda_{3,4,7,8}, \quad \Lambda_{1,2,5,6,7,8} = \Lambda_{1,2,5,6}\Lambda_{1,2,7,8}\Lambda_{5,6,7,8},\\ &\Lambda_{3,4,5,6,7,8} = \Lambda_{3,4,5,6}\Lambda_{3,4,7,8}\Lambda_{5,6,7,8}, \quad \Lambda_{1,2,3,4,5,6,7,8} = \Lambda_{1,2,3,4}\Lambda_{1,2,5,6}\Lambda_{1,2,7,8}\Lambda_{3,4,5,6}\Lambda_{3,4,7,8}\Lambda_{5,6,7,8}.\end{aligned} \qquad (4.18)$$

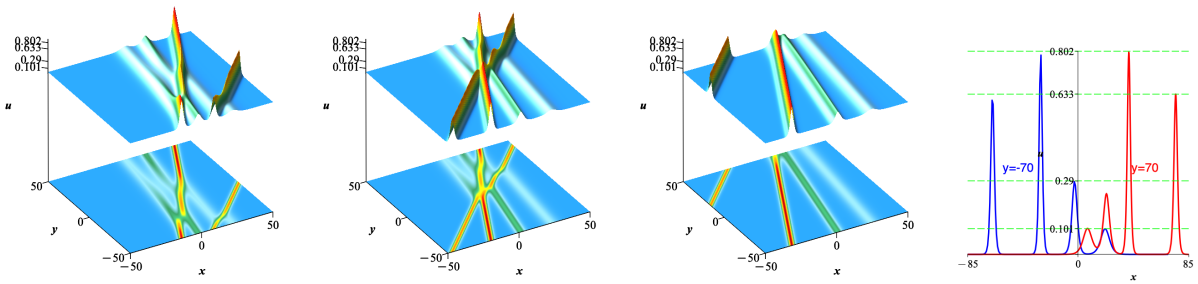

(a) $t = -3$ **(b)** $t = 0$ **(c)** $t = 4$ **(d)** $t = 0$

Figure 6. Evolution of a four-soliton solution (4.17) for parameters $\alpha = \frac{1}{2}, \beta = -2, k_1 = 1, k_2 = \frac{1}{8}, k_3 = \frac{1}{3}, k_4 = \frac{3}{7}, k_5 = \frac{2}{3}, k_6 = \frac{3}{5}, k_7 = \frac{1}{4}, k_8 = \frac{1}{5}, \zeta_1 = \zeta_2 = \zeta_3 = \zeta_4 = \zeta_5 = \zeta_6 = \zeta_7 = \zeta_8 = 0$. Three-dimensional surface plots of the wave profile $u(x, y, t)$ are shown at **(a)** $t = -3$, **(b)** $t = 0$, and **(c)** $t = 4$, demonstrating the interaction and stable propagation of four solitons. **(d)** shows the corresponding one-dimensional cross-sections at $t = 0$ for fixed $y = \pm 70$. The amplitudes of the first, second, third, and fourth solitons are 0.632, 0.2902, 0.802, and 0.101, respectively, propagating along the trajectories $x = -\frac{168101t}{10240} + \frac{301y}{320}$, $x = -\frac{33343t}{288120} + \frac{1781y}{8820}$, $x = -\frac{14529t}{5000} + \frac{409y}{900}$, and $x = -\frac{14529t}{5000} + \frac{409y}{900}$.

4.2. *Fission and fusion wave structures*

Fission and fusion wave phenomena represent important nonlinear interaction processes in integrable systems, where localized waves split into multiple structures or merge into a single coherent entity during evolution [32]. Such dynamics arise from the balance between nonlinearity and dispersion and provide insight into energy redistribution mechanisms in nonlinear media. In the present model, these behaviors can be analyzed through suitable parameter selections of the obtained analytical solutions, revealing rich interaction patterns beyond standard elastic soliton collisions.

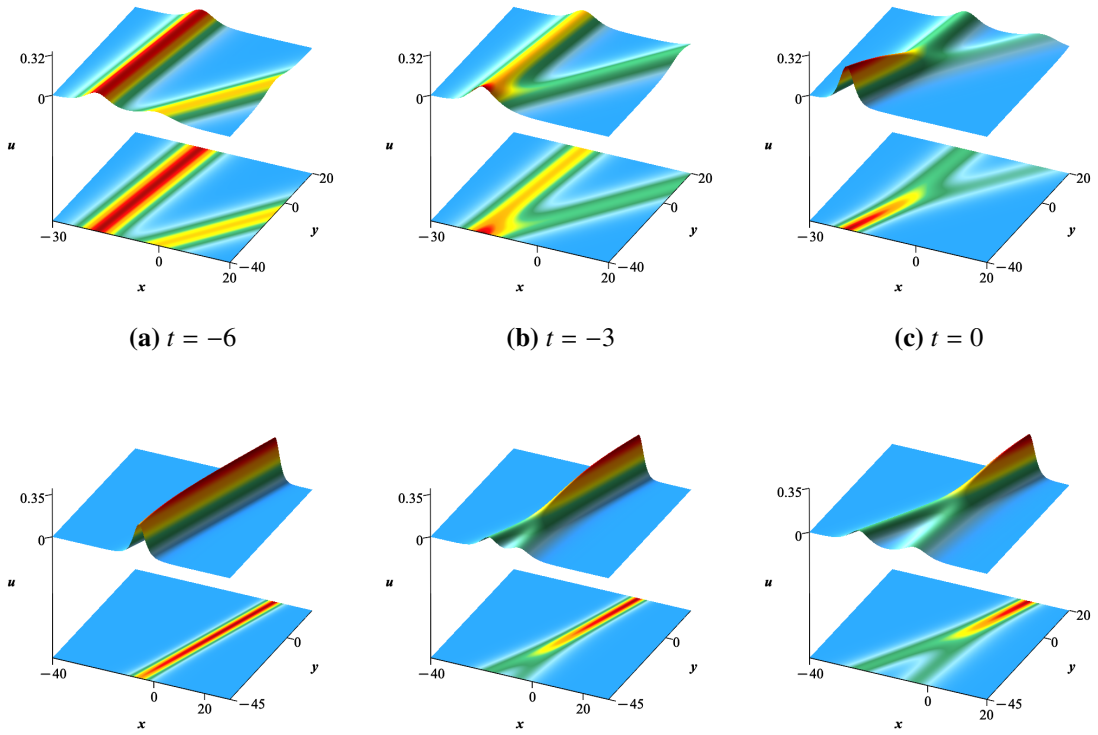

(a) $t = -6$ **(b)** $t = -3$ **(c)** $t = 0$

(d) $t = -6$ **(e)** $t = -3$ **(f)** $t = 0$

Figure 7. Y-type soliton interactions, exhibiting a distinct contrast to the standard two-soliton solution (4.15). Three-dimensional surface plots and corresponding contour projections of the wave profile $u(x, y, t)$ at selected time instances. The first row illustrates a fusion phenomenon in which two solitons merge into a single soliton over time, characterized by the following parameters: $\alpha = \frac{1}{2}, \beta = -2, k_1 = k_3 = \frac{1}{5}, k_2 = \frac{3}{5}, k_4 = \frac{1}{4}, \zeta_1 = \zeta_3 = 5, \zeta_2 = \zeta_4 = 0$. The second row illustrates a fission phenomenon in which a single soliton splits into two over time, characterized by the following parameters: $\alpha = \frac{1}{2}, \beta = -2, k_1 = -\frac{3}{5}, k_2 = k_4 = \frac{1}{7}, k_3 = \frac{1}{4}, \zeta_1 = \zeta_2 = \zeta_3 = \zeta_4 = 0$. Both panels demonstrate the spatial distribution and orientation of the resonance structures in the (x, y)-plane.

As shown in the N-soliton solution, there are $2N$ free parameters k_i $(i = 1, \ldots, 2N)$. By appropriately specifying these parameters, additional classes of nonlinear wave solutions can be constructed. We first examine τ_2 in (4.15). By imposing conditions that eliminate the coefficient of

the exponential term $e^{\phi_1+\phi_2+\phi_3+\phi_4}$, specifically $k_1 = k_3$ or $k_2 = k_4$, a Y-type (fissionable) soliton solution is obtained.

The corresponding solution dynamics are presented in Figure 7. Figure 7 (a) illustrates a fission process, whereas Figure 7 (b) depicts a fusion process.

In the three-soliton case, that is, for τ_3 in (4.16), when one of the following conditions is satisfied,

$$k_1 = k_3, \quad k_1 = k_4, \quad k_2 = k_3, \quad k_2 = k_4, \tag{4.19}$$

the resulting solution describes a mixed state consisting of one fissionable wave and one soliton wave. Figure 8 illustrates the interactions between a soliton and both fission and fusion waves.

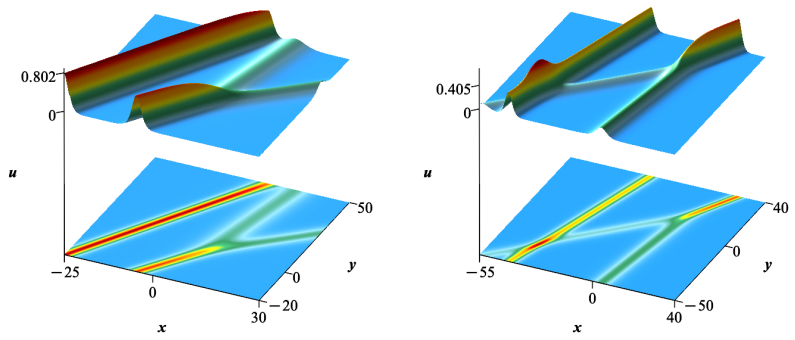

(a) **(b)**

Figure 8. Interaction between a line soliton and Y-type resonant waves, exhibiting a distinct contrast to the standard three-soliton solution (4.16). Three-dimensional surface plots and their corresponding contour projections of the wave profile $u(x, y, t)$ are shown at $t = 0$ for mixed-state solutions. **(a)** depicts the interaction of one line soliton with a fission wave for parameters $\alpha = \frac{1}{2}, \beta = -2, k_1 = \frac{1}{5}, k_2 = k_4 = \frac{3}{8}, k_3 = \frac{4}{5}, k_5 = \frac{2}{3}, k_6 = \frac{3}{5}, \zeta_1 = \zeta_2 = \zeta_3 = \zeta_4 = \zeta_6 = 0, \zeta_5 = 20$. **(b)** shows the interaction of one line soliton with a fusion wave for parameters $\alpha = \frac{1}{2}, \beta = -2, k_1 = \frac{1}{4}, k_2 = k_4 = \frac{1}{3}, k_3 = -\frac{4}{5}, k_5 = \frac{2}{5}, k_6 = \frac{1}{2}, \zeta_1 = \zeta_2 = \zeta_3 = \zeta_4 = \zeta_5 = 0, \zeta_6 = 25$. The plots demonstrate the stability and structural integrity of the solitons during these localized resonance interactions.

Moreover, by utilizing the τ_4 solution and appropriately specifying the free parameters, additional mixed solutions can be obtained, such as interactions between a soliton and a Y-type wave or between two Y-type solitons. Two representative cases are shown in Figure 9: one illustrating the interaction of two solitons with a fission wave, and the other depicting the interaction between a fission wave and a fusion wave.

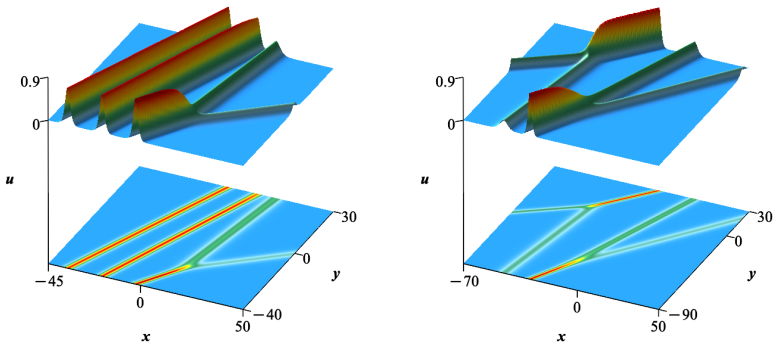

(a) **(b)**

Figure 9. Complex mixed-state solutions involving multiple line solitons and resonant Y-type waves, exhibiting a distinct contrast to the standard four-soliton solution (4.17). Surface plots and contour projections at $t = 0$ illustrate the spatial dynamics of higher-order interactions. **(a)** depicts the interaction of two line solitons with one fission wave for parameters $\alpha = \frac{1}{2}, \beta = -2, k_1 = k_3 = \frac{1}{3}, k_2 = 1, k_4 = \frac{3}{7}, k_5 = \frac{2}{3}, k_6 = \frac{3}{5}, k_7 = \frac{1}{2}, k_8 = \frac{3}{4}, \zeta_1 = \zeta_3 = -30, \zeta_2 = \zeta_4 = \zeta_6 = \zeta_8 = 0, \zeta_5 = 10, \zeta_7 = 20$. **(b)** depicts the interaction of one fission wave and one fusion wave for parameters $\alpha = \frac{1}{2}, \beta = -2, k_1 = k_3 = \frac{1}{3}, k_2 = -1, k_4 = \frac{3}{10}, k_5 = \frac{1}{6}, k_6 = k_8 = \frac{3}{5}, k_7 = \frac{3}{4}, \zeta_1 = \zeta_3 = 10, \zeta_2 = \zeta_5 = \zeta_6 = \zeta_7 = \zeta_4 = 10, \zeta_8 = -20$.

4.3. Breather solutions from the Pfaffian method perspective

Breather waves constitute localized oscillatory structures characterized by periodic behavior in either space or time while remaining spatially confined. They arise from the nonlinear superposition of soliton modes and reflect intermediate dynamics between solitary waves and periodic solutions [33].

To construct higher-order breather solutions of system (1.2) from the N-soliton solution (4.10), we set $N = 2M$ and impose appropriate constraints on the parameters k_i and ζ_i appearing in the N-soliton solution (4.10). These parameters are chosen to form complex-conjugate pairs as

$$\begin{aligned} k_{4h-3} &= k_{4h-1}^*, \quad k_{4h-2} = k_{4h}^*, \\ \zeta_{4h-3} &= \zeta_{4h-1}^*, \quad \zeta_{4h-2} = \zeta_{4h}^*, \end{aligned} \tag{4.20}$$

where k_h and ζ_h for $h = 1, 2, \ldots, M$ are arbitrary complex numbers and M is a positive integer. The symbol $(\cdot)^*$ denotes complex conjugation.

Under these constraints, the Mth-order breather solutions of the KdV-SKR-type equation (1.2) are given by

$$u = 2[\ln \tau_{2M}]_{xx}, \tag{4.21}$$

where the tau function τ_{2M} takes the form

$$\tau_{2M} = (1, 2, \ldots, 4h-2, 4h-1, 4h, \ldots, 4M), \tag{4.22}$$

with

$$(i,j) = c_{i,j}\frac{k_i - k_j}{k_i + k_j} + \frac{k_i - k_j}{k_i + k_j}e^{\phi_i+\phi_j}. \tag{4.23}$$

As illustrative examples, we consider the soliton solutions τ_2 in (4.15) and τ_4 in (4.17). By imposing the conditions outlined in Eq (4.20), one- and two-breather solutions can be constructed, respectively. The corresponding solutions are displayed in Figure 10.

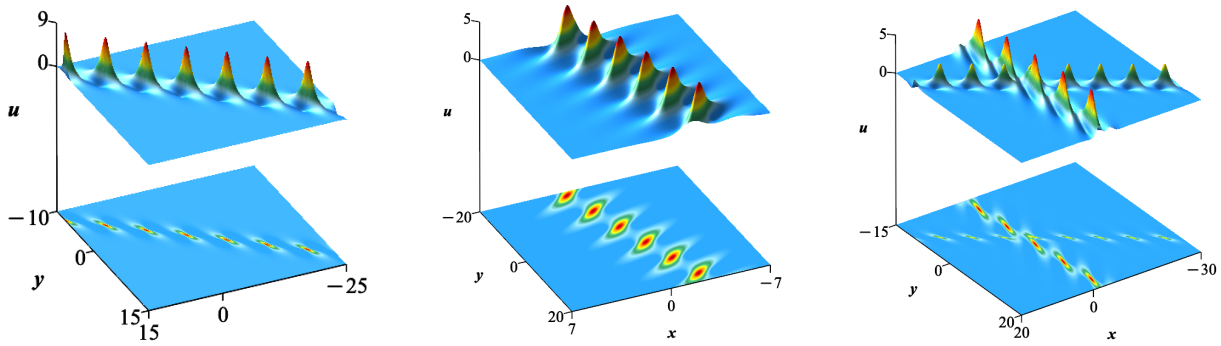

(a) **(b)** **(c)**

Figure 10. Evolution of one- and two-breather solutions and their mixed interactions, exhibiting a distinct contrast to standard two- and four-soliton solutions (4.15) and (4.17), respectively. **(a)** shows a single breather solution with parameters $\alpha = \frac{1}{2}, \beta = -2, k_1 = k_3^* = \frac{1}{6} + \frac{1}{7}\mathbf{i}, k_2 = k_4^* = \frac{1}{2} + \mathbf{i}, \zeta_1 = \zeta_2 = \zeta_3 = \zeta_4 = 0$. **(b)** shows a one-breather solution with parameters $\alpha = \frac{1}{5}, \beta = -\frac{2}{7}, k_1 = k_3^* = \frac{1}{8} + \frac{3}{7}\mathbf{i}, k_2 = k_4^* = \frac{3}{4} + \frac{1}{2}\mathbf{i}, \zeta_1 = \zeta_3 = -10, \zeta_2 = \zeta_4 = 10$. **(c)** illustrates a mixed state consisting of two breather waves with parameters $\alpha = \frac{1}{2}, \beta = -2, k_1 = k_3^* = \frac{2}{7} + \frac{1}{2}\mathbf{i}, k_2 = k_4^* = \frac{1}{5} + \frac{1}{2}\mathbf{i}, k_5 = k_7^* = \frac{1}{3} + \frac{1}{7}\mathbf{i}, k_6 = k_8 = \frac{1}{2} + \mathbf{i}, \zeta_1 = \zeta_2 = \zeta_3 = \zeta_4 = \zeta_5 = \zeta_6 = \zeta_7 = \zeta_8 = 0$ when $t = 0$.

To construct hybrid wave solutions of Eq (1.2) describing the interaction between $\mathcal{B}$ breather modes and $\mathcal{S}$ soliton modes, we employ the N-soliton solution (4.10) as the starting point. The interaction function (i, j) is taken to be identical to that defined in Eq (4.4). We then set

$$N = 2\mathcal{B} + \mathcal{S}$$

and impose the following constraints on the spectral parameters k_i and ζ_i:

$$\begin{aligned} &k_{4h-3} = k_{4h-1}^*, \quad k_{4h-2} = k_{4h}^*, \\ &\zeta_{4h-3} = \zeta_{4h-1}^*, \quad \zeta_{4h-2} = \zeta_{4h}^*, \\ &k_{4\mathcal{B}+l} = k_{4\mathcal{B}+l}^*, \quad \zeta_{4\mathcal{B}+l} = \zeta_{4\mathcal{B}+l}^*, \end{aligned} \tag{4.24}$$

where k_i and ζ_i are complex constants. Here, $\mathcal{B}$ and $\mathcal{S}$ are positive integers, with $h = 1, 2, \ldots, \mathcal{B}$ and $l = 1, 2, \ldots, 2\mathcal{S}$. The superscript $(\cdot)^*$ denotes complex conjugation.

Under these constraints, the hybrid solutions of (1.2) composed of $\mathcal{B}$ breather waves and $\mathcal{S}$ soliton waves can be written as

$$u = 2[\ln \tau_{2\mathcal{B}+\mathcal{S}}]_{xx}, \tag{4.25}$$

where the tau function $\tau_{2\mathcal{B}+\mathcal{S}}$ is defined by

$$\tau_{2\mathcal{B}+\mathcal{S}} = (1, 2, \ldots, 4h-2, 4h-1, 4h, \ldots, 4\mathcal{B}, 4\mathcal{B}+1, \ldots, 4\mathcal{B}+2\mathcal{S}) \tag{4.26}$$

and the interaction coefficients (i, j) are given by (4.23).

By applying the constraints outlined in Eq (4.24) and using the three- and four-soliton solutions (4.16) and (4.17), mixed solutions comprising soliton and breather waves can be readily constructed. Figure 11 illustrates these interactions: Figure 11 (a) shows the interaction between a single soliton and a breather wave, while Figure 11 (b) depicts the interaction of a breather with two soliton waves. Furthermore, by imposing an additional condition on τ_4, analogous to that used to generate Y-type solitons, a mixed solution consisting of one Y-type soliton and one breather wave can be obtained, as shown in Figure 11 (c).

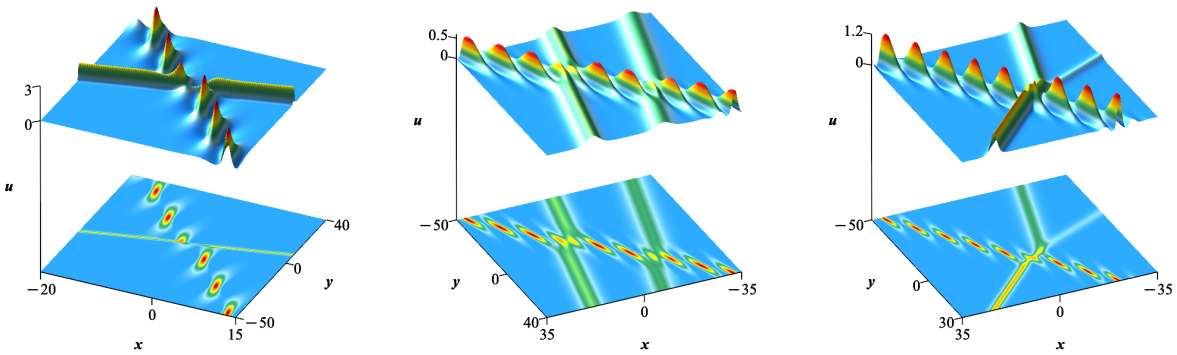

(a) **(b)** **(c)**

Figure 11. Mixed-state interactions between line solitons, breathers, and Y-type waves, exhibiting a distinct contrast to standard three- and four-soliton solutions (4.16) and (4.17). Three-dimensional surface plots and their corresponding contour projections of the wave profile $u(x, y, t)$ are illustrated at $t = 0$. **(a)** depicts the interaction of one line soliton with a breather wave for parameters $\alpha = \frac{1}{2}, \beta = -2, k_1 = k_3^* = \frac{2}{5} + \frac{1}{3}\mathbf{i}, k_2 = k_4^* = \frac{1}{5} + \frac{1}{2}\mathbf{i}, k_5 = -\frac{7}{5}, k_6 = -\frac{1}{3}, \zeta_1 = \zeta_2 = \zeta_3 = \zeta_4 = \zeta_5 = \zeta_6 = 0$. **(b)** shows the interaction between two line solitons and one breather wave for parameters $\alpha = \frac{1}{2}, \beta = -2, k_1 = k_3^* = \frac{2}{9} + \frac{1}{2}\mathbf{i}, k_2 = k_4^* = \frac{1}{8} + \frac{1}{2}\mathbf{i}, k_5 = \frac{1}{3}, k_6 = \frac{1}{3}, k_7 = \frac{1}{8}, k_8 = \frac{3}{7}, \zeta_1 = \zeta_2 = \zeta_3 = \zeta_4 = \zeta_5 = \zeta_6 = \zeta_8 = 0, \zeta_7 = 10$. **(c)** illustrates the interaction of a breather wave with a fission wave for parameters $\alpha = \frac{1}{2}, \beta = -2, k_1 = k_3^* = \frac{2}{7} + \frac{1}{2}\mathbf{i}, k_2 = k_4^* = \frac{1}{5} + \frac{1}{2}\mathbf{i}, k_5 = k_7 = \frac{1}{2}, k_6 = -1, k_8 = \frac{3}{10}, \zeta_1 = \zeta_2 = \zeta_3 = \zeta_4 = \zeta_5 = \zeta_6 = \zeta_8 = 0, \zeta_7 = 5$.

4.4. Lump solutions from the Pfaffian method perspective

In this section, we construct multi-lump solutions for the KdV–SKR-type model using the Pfaffian method. These multi-rational solutions, often called lumps, are localized waveforms characterized by compact, rational structures with distinct peaks.

In general, the Pfaffian solution of the equation is defined as

$$u = 2[\ln \tau_N]_{xx}, \tag{4.27}$$

where τ_N is given by

$$\tau_N = (1, 2, 3, \ldots, 2N), \tag{4.28}$$

with entries

$$(i, j) = c_{i,j} + \int^x D_x\psi_i.\psi_j dx, \quad c_{i,j} = -c_{j,i}. \tag{4.29}$$

Our aim is to derive explicit rational solutions of Eq (1.2) by appropriately selecting the functions ψ_i that appear in the Pfaffian entries (4.28). To accomplish this, we choose the functions

$$\psi_i = \mathscr{A}_i e^{\phi_i}, \quad \mathscr{A}_i = \sum_{p=0}^{n_i} c_{i,p}\partial_{k_i}^{n_i-p}, \tag{4.30}$$

where ϕ_i's are defined as

$$\phi_i = k_i x + \left(\frac{\alpha k_i}{5\beta} - k_i^3\right)y + \Big(- \frac{k_i\alpha^2}{5\beta} - k_i\alpha + 2\alpha k_i^3 - 9\beta k_i^5\Big)t + \zeta_i, \tag{4.31}$$

where $c_{i,p}$ are arbitrary complex constants and n_i are non-negative integers. It is straightforward to verify that these functions satisfy the differential system (4.6). Using ψ_i, the Pfaffian entries (i, j) take the form

$$(i, j) = e^{\phi_i+\phi_j}\sum_{p=0}^{n_i} c_{i,p}(\partial_{k_i} + \phi_{i,k_i})^{n_i-p}\sum_{q=0}^{n_j} c_{j,q}(\partial_{k_j} + \phi_{j,k_j})^{n_j-q}\frac{k_i - k_j}{k_i + k_j}, \tag{4.32}$$

with $\phi_{i,k_i} = \partial_{k_i}\phi_i$.

Each lump (i-th lump) in the solution is uniquely associated with a pair of wave numbers (k_i, k_{i+N}) for $i = 1, \ldots, N$. These parameters not only determine the amplitude and spatial position of each lump but also control the overall shape and propagation characteristics of the corresponding wave. In particular, they specify:

- The trajectory of each lump, which is governed by

$$y = \frac{T_1}{T_2}, \tag{4.33}$$

where

$$\begin{aligned}
T_1 = {} & 5\Big(+ c_{2,1}\left(6k_{i+N}k_i^2 - 6k_i^3 + k_i - k_{i+N}\right) + 12(k_i^2 - k_ik_{i+N} + k_{i+N}^2) - 2\Big)\beta\alpha \\
& + 225\Big(c_{1,1}\left(k_{i+N}^5 - k_ik_{i+N}^4\right) + c_{2,1}\left(k_i^5 - k_i^4k_{i+N}\right) + 2(k_{i+N}k_i^3 - k_i^2k_{i+N}^2 + k_ik_{i+N}^3 - k_i^4 - k_{i+N}^4)\Big)\beta^2 \\
& \Big(c_{1,1}(k_{i+N} - k_i) + c_{2,1}(k_i - k_{i+N}) - 2\Big)\alpha^2 + 225\beta(k_i - k_{i+N})^2(k_i + k_{i+N})\left(\beta k_i^2 + \beta k_{i+N}^2 - \frac{2}{15}\alpha\right)x, \\
& + 5\beta\alpha\Big(c_{1,1}\left(k_i\left(6k_{i+N}^2 - 1\right) - 6k_{i+N}^3 + k_{i+N}\right)\Big), \\
T_2 = {} & 675(k_i + k_{i+N})(k_i - k_{i+N})^2\left(\beta^2k_i^2k_{i+N}^2 - \frac{\left(k_i^2 + k_{i+N}^2 + \frac{1}{3}\right)\alpha\beta}{15} + \frac{\alpha^2}{225}\right).
\end{aligned}$$

- The amplitude of the i-th lump is given by

$$A_L := \frac{2\left(k_i^2 - k_{i+N}^2\right)^2}{k_i^2 + k_{i+N}^2}. \tag{4.34}$$

- The velocity vector of each wave is obtained by

$$\begin{pmatrix} V_x \\ V_y \end{pmatrix} = \begin{pmatrix} \alpha\left(3k_i^2 + 3k_{i+N}^2 + 1\right) - 45\beta k_i^2 k_{i+N}^2 - \frac{\alpha^2}{5\beta} \\ 2\alpha - 15\beta\left(k_i^2 + k_{i+N}^2\right) \end{pmatrix}. \tag{4.35}$$

- Moreover, the resulting solutions satisfy the natural decay conditions

$$\lim_{x\to\infty} u = \lim_{y\to\infty} u = \lim_{t\to\infty} u = 0. \tag{4.36}$$

One-lump: For the simplest case $N = 1$ in (4.28) and $n_1 = n_2 = 1$, the Pfaffian reduces to

$$\begin{aligned} \tau_1 = (1,2) &= e^{\phi_1+\phi_2} \sum_{p=0}^{1} r_{1p}(\partial_{k_1} + \phi_{1,k_1})^{1-p} \sum_{q=0}^{1} r_{2q}(\partial_{k_2} + \phi_{2,k_2})^{1-q} \frac{k_1 - k_2}{k_1 + k_2} \\ &= e^{\phi_1+\phi_2} \frac{k_1 - k_2}{k_1 + k_2} \left[\left(\phi_{1,k_1} + r_{11} + \frac{2k_2}{k_1^2 - k_2^2}\right)\left(\phi_{2,k_2} + r_{21} - \frac{2k_1}{k_1^2 - k_2^2}\right) + \frac{2(k_1^2 + k_2^2)}{(k_1^2 - k_2^2)^2}\right]. \end{aligned} \tag{4.37}$$

Then, the corresponding one-lump solution is

$$u = 2[\ln \tau_1']_{xx}, \tag{4.38}$$

where

$$\tau_1' = \frac{k_1 - k_2}{k_1 + k_2} \left[\left(\phi_{1,k_1} + r_{11} + \frac{2k_2}{k_1^2 - k_2^2}\right)\left(\phi_{2,k_2} + r_{21} - \frac{2k_1}{k_1^2 - k_2^2}\right) + \frac{2(k_1^2 + k_2^2)}{(k_1^2 - k_2^2)^2}\right].$$

In this expression, we set $k_1 = k_2^*$ and $r_{11} = r_{21}^*$. Note that the exponential factor $e^{\phi_1+\phi_2}$ can be omitted, as it does not influence the resulting solution. Figure 12 illustrates the evolution dynamics of the lump wave, along with its amplitude, velocity, and trajectory.

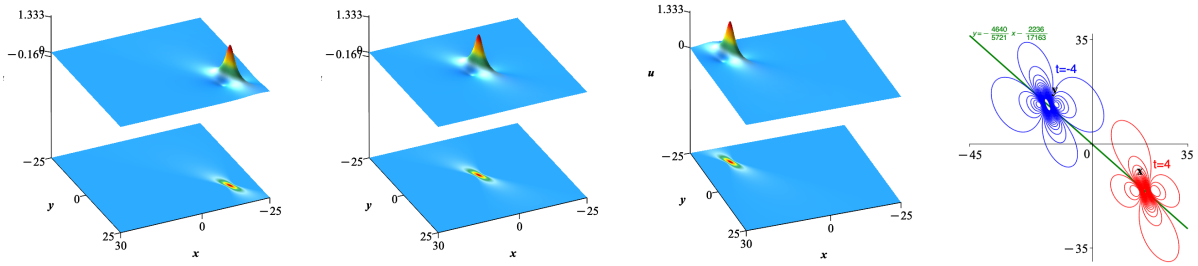

(a) $t = -4$ **(b)** $t = 0$ **(c)** $t = 4$ **(d)**

Figure 12. Evolution and trajectory of a one-lump solution (4.38). Three-dimensional surface plots and their corresponding contour projections of the wave profile $u(x, y, t)$ are shown at **(a)** $t = -4$, **(b)** $t = 0$, and **(c)** $t = 4$. The parameters are specified as $\alpha = 1, \beta = -1, c_{1,1} = c_{2,1} = 1, k_1 = k_2^* = \frac{1}{4} + \frac{1}{2}\mathbf{i}$. The maximum amplitude of the wave is constant at $\frac{4}{3}$. **(d)** illustrates the corresponding two-dimensional contour plots at $t = -4$ (blue) and $t = 4$ (red), clearly demonstrating the linear motion of the lump wave. The trajectory of the wave is given by the line $y = -\frac{4640x}{5721} - \frac{2236}{17163}$, with characteristic velocities $V_x = \frac{5721}{1280}$ and $V_y = -\frac{29}{8}$.

We now turn to the case where $N > 1$. To identify the Pfaffian entries that satisfy the required antisymmetry condition, it is necessary to impose the constraint that certain indices are equal, as described in Eq (4.32). For instance, when $N = 2$ and the relevant parameters take the simplest nontrivial values, the corresponding τ-function can be explicitly constructed using the Pfaffian formalism as

$$\tau_2 = (1,2,3,4) = (1,2)(3,4) - (1,3)(2,4) + (1,4)(2,3) = e^{\phi_1+\phi_2+\phi_3+\phi_4}\tau_2', \tag{4.39}$$

where

$$\tau_2' = (1',2')(3',4') - (1',3')(2',4') + (1',4')(2',3'), \tag{4.40}$$

with entries

$$(i',j') = \frac{k_i - k_j}{k_i + k_j}\left[\left(\phi_{i,k_i} + c_{i,1} + \frac{2k_j}{k_i^2 - k_j^2}\right)\left(\phi_{j,k_j} + c_{j,1} - \frac{2k_i}{k_i^2 - k_j^2}\right) + \frac{2(k_i^2 + k_j^2)}{(k_i^2 - k_j^2)^2}\right], \tag{4.41}$$

and $c_{i,1}$ and $c_{j,1}$ $(i = 1, \ldots, 4)$ are arbitrary complex parameters. From this construction, the two-lump solution emerges naturally as

$$u = 2[\ln \tau_2']_{xx}. \tag{4.42}$$

Each entry in the Pfaffian is determined by a combination of exponential terms and free complex parameters, which can be adjusted to produce a variety of solution behaviors. By differentiating the logarithm of the resulting τ-function, one obtains the explicit expression for the two-lump wave. Figure 13 depicts the temporal evolution of the two-lump solution for a specific choice of conjugate parameters. The dynamics exhibit two distinct peaks, each following its own trajectory with characteristic velocities and amplitudes, as indicated in the figure.

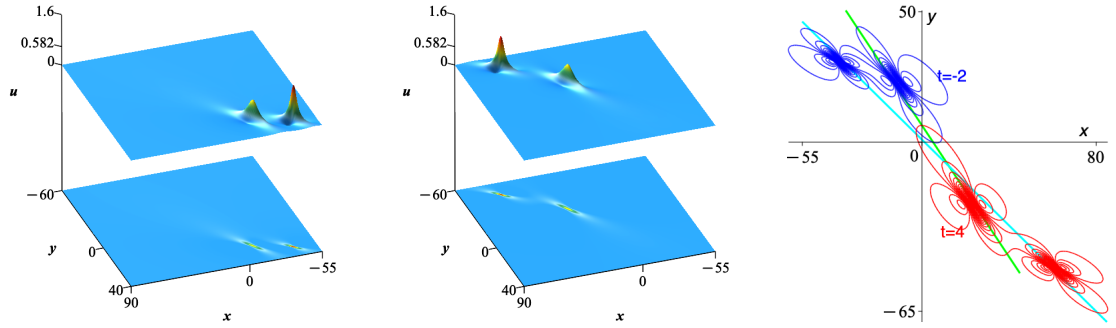

(a) $t = -2$ **(b)** $t = 4$ **(c)**

Figure 13. Evolution and interaction of a two-lump solution (4.42). Three-dimensional surface plots of the wave profile $u(x, y, t)$ and their corresponding contour projections are shown at **(a)** $t = -2$ and **(b)** $t = 4$. The parameters are set as $\alpha = 1, \beta = -1, c_{1,1} = c_{4,1} = -3, c_{2,1} = c_{3,1} = 1, k_1 = k_4^* = -\frac{2}{11} + \frac{3}{5}\mathbf{i}, k_2 = k_3^* = \frac{1}{4} + \frac{3}{4}\mathbf{i}$. The amplitude of the first wave is $\frac{576}{989}$ and the second wave is $\frac{9}{8}$. **(c)** displays the corresponding two-dimensional contour plots at $t = -2$ (blue) and $t = 4$ (red). The trajectory of the first wave is defined by $y = -\frac{14290100x}{11329569} + \frac{818822675}{2447186904}$ with velocities $V_x = 6.19$ and $V_y = -7.808$, while the second wave follows the trajectory $y = -\frac{4160x}{5049} + \frac{936002}{136323}$ with velocities $V_x = 15.778$ and $V_y = -13$.

From the foregoing discussion, it follows that the N-lump solution can be represented in terms of the Pfaffian solution given in Eq (4.28).

Remark 1. *It is important to clarify the relation between the present model and the KdV–SKR equation. By introducing the scaling transformation*

$$x \to x - \alpha t, \quad t \to t, \quad y \to y, \tag{4.43}$$

the KdV–SKR-type equation (1.1) *considered here reduces to the original KdV–SKR equation. Consequently, all soliton and lump solutions derived in Section 3 are consistent with the solutions reported in [26, 34].*

However, to the best of our knowledge, Pfaffian solutions for the original KdV–SKR equation have not been reported in the existing literature. We constructed Pfaffian solutions for the proposed equation and showed that, after applying the coordinate scaling (4.43)*, the obtained Pfaffian structures also generated solutions of the original KdV–SKR equation. Therefore, the present formulation not only reproduces known results but also provides a new Pfaffian representation that extends the solution structures of the model.*

The KdV–SKR-type equation considered in this work belongs to a class of higher-order nonlinear evolution equations that extend the classical KdV model by incorporating additional dispersive and nonlinear effects. Such models arise in more accurate descriptions of wave propagation in shallow water, plasma physics, and nonlinear optical media, particularly in regimes where higher-order corrections cannot be neglected. In these contexts, soliton solutions represent stable localized wave packets, while lump and breather solutions correspond to rationally localized and oscillatory

structures, respectively. The multi-wave interaction patterns obtained in this study, including resonant (Y-type) structures and breather dynamics, provide insight into complex energy exchange and stability properties of nonlinear waves. Therefore, the analytical results presented here contribute to a deeper theoretical understanding of wave phenomena in higher-order dispersive systems with potential relevance to realistic physical models.

5. Conclusions

In this work, we investigated the integrability and nonlinear multi-wave dynamics of a KdV–SKR-type equation through analytical methods. The equation's integrability was verified through Painlevé analysis, after which its bilinear representation was derived using the BP method. Based on this bilinear form, multi-soliton solutions were constructed using the simplified Hirota method, and the corresponding multi-lump solutions were obtained by applying the long-wave limit procedure.

Furthermore, a Pfaffian framework was developed to provide a compact and unified representation of the solutions. This approach allowed the systematic construction of general N-soliton configurations as well as multi-lump structures, offering a more efficient algebraic description of nonlinear interactions. Through appropriate parameter selections, various complex wave phenomena, including fission–fusion processes and breather dynamics, were obtained and analyzed.

An important observation concerns the relation between the considered model and the original KdV–SKR equation. Through a suitable coordinate scaling, the present equation can be reduced to the standard form, showing that the Pfaffian formulation developed here provides a new representation that extends the known solution structure, demonstrating that the constructed Pfaffian solutions also generate valid solutions for the original KdV–SKR equation.

The results demonstrate that the proposed formulation enriches the analytical solution space of the equation and deepens the understanding of nonlinear wave interactions in integrable KdV–SKR-type models. Future work may focus on extending the present approach to higher-dimensional models, variable-coefficient systems, and related nonlinear evolution equations. In addition, an interesting direction is the development of a statistical framework based on soliton turbulence, originally introduced by Zakharov [35] and recently reviewed by Didenkulova et al. [36]. Given the integrability and rich multi-soliton structures obtained here, the present model may provide a suitable setting for constructing a soliton gas description and its associated kinetic theory, which we leave for future investigation.

Author contributions

Conceptualization, methodology, investigation, formal analysis, visualization, validation, and writing review and editing, M.M., K.H., F.A., E.H. and S.S.; Software, data curation, and writing original draft preparation, M.M., K.H. and S.S.; Resources, supervision, and project administration, K.H. and S.S.; Funding acquisition, S.S. All authors have read and agreed to the published version of the manuscript.

Use of Generative-AI tools declaration

During the preparation of this manuscript, the authors used ChatGPT to enhance the readability and clarity of the language. After using this tool, the authors carefully reviewed and edited the content as necessary and assume full responsibility for the final published work.

Acknowledgments

This research budget was allocated by National Science, Research and Innovation Fund (NSRF), and King Mongkut's University of Technology North Bangkok (Project no. KMUTNB-FF-69-B-17).

Conflict of interest

The authors declare that they have no conflicts of interest in this paper.

References

1. A. M. Wazwaz, Multiple soliton solutions and other scientific solutions for a new Painlevé integrable fifth-order equation, *Chaos Soliton. Fract.*, **196** (2025), 116307. https://doi.org/10.1016/j.chaos.2025.116307
2. X. J He, X. Lü, *M*-lump solution, soliton solution and rational solution to a (3+1)-dimensional nonlinear model, *Math. Comput. Simulat.*, **197** (2022), 327–340. https://doi.org/10.1016/j.matcom.2022.02.014
3. K. J. Wang, K. H. Yan, S. Li, Multi-rogue wave, generalized breathers wave, bell shape and singular wave solutions to the (3+1)-dimensional Yu–Toda–Sasa–Fukuyama equation, *Math. Methods Appl. Sci.*, 2026. https://doi.org/10.1002/mma.70663
4. F. Shi, M. Qi, K. J. Wang, Multi-kink solitons, resonant soliton molecules and multi-lumps solutions to the (3+1)-dimensional shallow water wave equation, *Mod. Phys. Lett. B*, **39** (2025), 2550039. https://doi.org/10.1142/S0217984925500393
5. C. Li, X. Liu, B. F. Feng, Pfaffian solution for dark-dark soliton to the coupled complex modified Korteweg–de Vries equation, *Wave Motion*, **139** (2025), 103611. https://doi.org/10.1016/j.wavemoti.2025.103611
6. K. Hosseini, F. Alizadeh, S. Sirisubtawee, C. Kamthorncharoen, S. Kheybari, K. Dehingia, Integrability, Hirota *D*-operator expression, multi solitons, breather wave, and complexiton of a generalized Korteweg-de Vries–Caudrey Dodd Gibbon equation, *AIMS Mathematics*, **10** (2025), 5248–5263. https://doi.org/10.3934/math.2025242
7. C. Zhang, Z. Zhao, J. Yue, Wronskian solutions, bilinear Bäcklund transformation, quasi-periodic waves and asymptotic behaviors for a (3+1)-dimensional generalized Kadomtsev–Petviashvili equation, *Wave Motion*, **128** (2024), 103327. https://doi.org/10.1016/j.wavemoti.2024.103327
8. M. V. Flamarion, E. Pelinovsky, Emergence of champion solitons from two-solitary-wave interactions in the fourth-order generalized Korteweg–de Vries equation, *Chaos Soliton. Fract.*, **208** (2026), 118271. https://doi.org/10.1016/j.chaos.2026.118271

9. J. Li, J. Wei, X. Wang, A generalized massive Thirring model: Darboux transformation, higher-order soliton and rogue wave solutions, *Nonlinear Dyn.*, **114** (2026), 6. https://doi.org/10.1007/s11071-025-11878-7
10. X. Y. Gao, Hetero-and auto-Bäcklund transformations for a generalized Broer–Kaup–Kupershmidt system in shallow water, *Chaos Soliton. Fract.*, **208** (2026), 118301. https://doi.org/10.1016/j.chaos.2026.118301
11. K. J. Wang, Exploring exact wave solutions of the Cahn–Allen equation via a novel Bernoulli sub-equation neural networks method, *Mod. Phys. Lett. B*, **40** (2026), 2650062. https://doi.org/10.1142/S0217984926500624
12. J. Weiss, M. Tabor, G. Carnevale, The Painleve property for partial differential equations, *J. Math. Phys.*, **24** (1983), 522–526. https://doi.org/10.1063/1.525721
13. L. Yan, N. Raza, N. Jannat, H. M. Baskonus, G. A. Basendwah, Painlevé analysis, Painlevé–Bäcklund, multiple regular and singular kink solutions of dynamical thermopherotic equation drafting wrinkle propagation, *Opt. Quant. Electron.*, **56** (2024), 689. https://doi.org/10.1007/s11082-024-06352-4
14. Y. Q. Chen, B. Tian, Q. X. Qu, C. C. Wei, D. Y. Yang, Painlevé integrable property, bilinear form, Bäcklund transformation, kink and soliton solutions of a (2+1)-dimensional variable-coefficient general combined fourth-order soliton equation in a fluid or plasma, *J. Appl. Anal. Comput.*, **14** (2024), 742–759. https://doi.org/10.11948/20230056
15. S. Bochner, B. Jessen, Distribution functions and positive-definite functions, *Ann. Math.*, **35** (1934), 252–257. https://doi.org/10.2307/1968430
16. F. Lambert, I. Loris, J. Springael, R. Willer, On a direct bilinearization method: Kaup's higher-order water wave equation as a modified nonlocal Boussinesq equation, *J. Phys. A: Math. Gen.*, **27** (1994), 5325. https://doi.org/10.1088/0305-4470/27/15/028
17. X. Hu, Y. Chen, A direct procedure on the integrability of nonisospectral and variable-coefficient MKdV equation, *J. Nonlinear Math. Phys.*, **19** (2012), 16–26. https://doi.org/10.1142/S1402925112500027
18. Y. Wang, Y. Chen, Bell polynomials approach for two higher-order KdV-type equations in fluids, *Nonlinear Anal.-Real*, **31** (2016), 533–551. https://doi.org/10.1016/j.nonrwa.2016.03.005
19. X. Hao, Z. Cheng, Integrability and exact solutions of the non-isospectral KP equation with binary Bell polynomials approach, *Eur. Phys. J. Plus*, **140** (2025), 661. https://doi.org/10.1140/epjp/s13360-025-06602-8
20. K. J. Wang, K. H. Yan, J. Cheng, Y. B. Zheng, F. Shi, H. W. Zhu, et al., Bilinear form, Bäcklund transformation to the Kairat-II-X-extended equation: N-soliton, anti-kink soliton, novel soliton molecule, multi-lump and travelling wave solutions, *Mod. Phys. Lett. B*, **40** (2026), 2650057. https://doi.org/10.1142/S0217984926500570
21. L. Na, Bäcklund transformation and multi-soliton solutions for the (3+1)-dimensional BKP equation with Bell polynomials and symbolic computation, *Nonlinear Dyn.*, **82** (2015), 311–318. https://doi.org/10.1007/s11071-015-2159-1
22. T. T. Zhang, P. L. Ma, M. J. Xu, X. Y. Zhang, S. F. Tian, On Bell polynomials approach to the integrability of a (3+1)-dimensional generalized Kadomtsev–Petviashvili equation, *Mod. Phys. Lett. B*, **29** (2015), 1550051. https://doi.org/10.1142/S0217984915500517

23. R. Hirota, *The direct method in soliton theory*, Cambridge university press, 2004. https://doi.org/10.1017/CBO9780511543043
24. B. Yapiskan, Pfaffian solutions to the Hirota–Satsuma–Ito equation, *Eur. Phys. J. Plus*, **140** (2025), 744. https://doi.org/10.1140/epjp/s13360-025-06670-w
25. L. Hu, Y. T. Gao, S. L. Jia, J. J. Su, G. F. Deng, Solitons for the (2+1)-dimensional Boiti–Leon–Manna–Pempinelli equation for an irrotational incompressible fluid via the Pfaffian technique, *Mod. Phys. Lett. B*, **33** (2019), 1950376. https://doi.org/10.1142/S0217984919503767
26. C. Zhu, C. X. Long, Y. T. Zhou, P. F. Wei, B. Ren, W. L. Wang, Dynamics of multi-solitons, multi-lumps and hybrid solutions in (2+1)-dimensional Korteweg–de Vries–Sawada–Kotera–Ramani equation, *Results Phys.*, **34** (2022), 105248. https://doi.org/10.1016/j.rinp.2022.105248
27. B. Ren, J. Lin, W. L. Wang, Painlevé analysis, infinite dimensional symmetry group and symmetry reductions for the (2+1)-dimensional Korteweg–de Vries–Sawada–Kotera–Ramani equation, *Commun. Theor. Phys.*, **75** (2023), 085006. https://doi.org/10.1088/1572-9494/ace350
28. P. F. Wei, C. X. Long, C. Zhu, Y. T. Zhou, H. Z. Yu, B. Ren, Soliton molecules, multi-breathers and hybrid solutions in (2+1)-dimensional Korteweg–de Vries–Sawada–Kotera–Ramani equation, *Chaos Soliton. Fract.*, **158** (2022), 112062. https://doi.org/10.1016/j.chaos.2022.112062
29. W. Chen, L. Tang, L. Tian, New interaction solutions of the KdV–Sawada–Kotera–Ramani equation in various dimensions, *Phys. Scr.*, **98** (2023), 055217. https://doi.org/10.1088/1402-4896/acc141
30. M. Madadi, M. Inc, H. Bicer, E. C. Aslan, Exploring nonlinear wave dynamics through an extended (2+1)-dimensional nonlinear evolution equation: Integrability and Pfaffian solutions, *Wave Motion*, **142** (2026), 103700. https://doi.org/10.1016/j.wavemoti.2026.103700
31. Y. Shen, B. Tian, C. D. Cheng, T. Y. Zhou, Pfaffian solutions and nonlinear waves of a (3+1)-dimensional generalized Konopelchenko–Dubrovsky–Kaup–Kupershmidt system in fluid mechanics, *Phys. Fluids*, **35** (2023), 025103. https://doi.org/10.1063/5.0135174
32. E. Asadi, K. Hosseini, M. Madadi, Superposition of soliton, breather and lump waves in a non-painlevé integrabale extension of the Boiti–Leon–Manna–Pempinelli equation, *Phys. Scr.*, **99** (2024), 125242. https://doi.org/10.1088/1402-4896/ad8f74
33. J. Wang, Y. Li, J. Wei, Solitons, breathers and rogue waves in a reverse time nonlocal generalized nonlinear Schrödinger equation with four-wave mixing effect, *Nonlinear Dyn.*, **113** (2025), 18485–18502. https://doi.org/10.1007/s11071-025-11129-9
34. H. Wang, S. Tian, T. Zhang, Nonlinear wave transitions and their mechanisms of the (2+ 1)-dimensional Korteweg–de Vries–Sawada–Kotera–Ramani equation, *Acta Math. Sci.*, **45** (2025), 1405–1437. https://doi.org/10.1007/s10473-025-0410-5
35. V. E. Zakharov, Kinetic equation for solitons, *Sov. Phys. JETP*, **33** (1971), 538–541.
36. E. Didenkulova, M. V. Flamarion, E. Pelinovsky, KdV-like soliton gas: Similarity and difference in integrable and non-integrable models, *Physica D*, **481** (2025), 134815. https://doi.org/10.1016/j.physd.2025.134815